Title: Atlas of innate immune responses to experimental cholera and IL22 treatment demonstrates protection by mucus-secreting cells

Authors: Masataka Suzuki[1]§, Yuko Hasegawa[1]†§, Hailong Zhang[1]‡, Matthew K. Waldor[1]*

Affiliations:

1. Department of Microbiology, Harvard Medical School, Division of Infectious Diseases, Brigham & Women's Hospital, Howard Hughes Medical Institute, Boston, MA 02115.

†. Current affiliation: Molecular Biology and Genetics, Cornell University, Ithaca, NY, 14853.

‡. Current affiliation: Medical University of South Carolina, Charleston, SC 29425.

§ These authors contributed equally

* Corresponding author. Email: mwaldor@research.bwh.harvard.edu

Abstract: The diarrheal disease cholera remains a global threat. However, knowledge of the innate immune defenses in the small intestine that protect against the causative agent, *Vibrio cholerae,* is limited. Here, single-cell RNA-sequencing of epithelial and immune cells mapped the patterns of gene expression in the infant mouse small intestine, as well as the transcriptional response to *V. cholerae* infection and treatment with an IL22 Fc-fusion protein. Infection increased the abundance of an enterocyte subtype that highly expressed defense-associated functions and stimulated production of IL22, a cytokine linked to epithelial integrity, from group 3 innate lymphoid cells. Administration of IL22Fc increased production of vibriocidal Reg3β from enterocytes and the abundance of secretory lineage and Muc2-producing goblet cells, which secreted mucus into the intestinal crypts, impairing *V. cholerae* association with the epithelium. These IL22-mediated responses limited *V. cholerae* intestinal colonization and protected mice from diarrhea and death. These observations suggest enterocyte specialization in mucosal defense, identify mechanisms of IL22-mediated protection, and point to host-directed approaches for cholera therapeutics.

Main Text:

Introduction

Vibrio cholerae, the cholera pathogen, infects several million people and causes tens of thousands of deaths annually, particularly in low- and middle-income countries in south Asia and Africa[1]. Cholera patients can lose many liters of diarrheal fluid within hours and die from dehydration without proper treatment[2]. *V. cholerae* is a curved, highly motile Gram-negative rod that associates with the epithelium of the human small intestine (SI), the site of colonization. Various *V. cholerae* genes and processes, including its Tcp pilus along with flagellar-based motility are important for intestinal colonization[3]. While replicating along the epithelium, the pathogen secretes cholera toxin, whose activities largely account for the secretory diarrhea characteristic of cholera.

Knowledge of adaptive immune responses to natural and experimental *V. cholerae* infection in humans has expanded in recent years[4]. Infection leads to the generation of protective antibody responses that can limit intestinal colonization and diarrhea[5]. However, despite more than a century of studies of cholera pathogenesis, the understanding of epithelial and innate immune responses to *V. cholerae* infection in the small intestine is limited[6–8]. Epithelial cells represent a critical barrier preventing pathogens or commensal bacteria from entering host tissues, and these cells produce physical (e.g., mucus) and chemical (e.g., reactive oxygen species, antimicrobial peptides) obstacles that impede microbial invasion of deeper tissues[6]; epithelial cells also initiate immune responses when the epithelial barrier is compromised[9]. In cholera naïve individuals, such innate responses are likely to be critical determinants of survival given that severe cholera can kill infected individuals within a day of infection, before adaptive immune responses are generated[2].

Modeling human pathogenesis, *V. cholerae* robustly colonizes the small intestine (SI) of infant mice without antibiotic pre-treatment. Furthermore, colonization of the infant mouse SI depends on the Tcp pathogenicity island, as is the case in humans[10]. Here, we characterized intestinal epithelial and immune cell responses to *V. cholerae* infection in infant mice using single-cell RNA sequencing (scRNA-seq). Our findings uncover patterns of mucosal innate defense and reveal that IL22 therapy shifts stem cell differentiation toward the secretory lineage, which protects against infection by impairing pathogen association with the epithelium. These findings could point to new approaches for cholera treatment.

Results

V. cholerae infection triggers antimicrobial responses in intestinal epithelial cells

scRNA-seq analysis of epithelial cells harvested from the SI of postnatal day 5 (P5) infant mice revealed 15 cell clusters, including various enterocyte subtypes, goblet cells, and enteroendocrine cells (Fig. 1ab, Extended Data Fig. 1ab, Supplementary Table 1). The expression profiles in the 11 enterocyte clusters and stem cells likely distinguish where they are located along the crypt-villus axis[13] (Extended Data Fig. 1c). However, Paneth and tuft cells were not detected (Extended Data Fig. 1d), revealing the developmental immaturity of the epithelial defense system in P5 mice[11].

V. cholerae infection altered the transcriptional profiles in nearly all clusters of SI epithelial cells, particularly in the distal SI, where the pathogen burden is 10-100x greater than in

the proximal SI[12] (Extended Data Fig. 2a, Supplementary Table 2, 3). Pathway analyses showed prominent upregulation of inflammatory signaling and hypoxia pathways across almost all epithelial cell clusters (Fig. 1cd, Extended Data Fig. 2b). There were also cell type-specific infection-induced perturbations, such as in metabolic pathways (Fig. 1d, Extended Data Fig. 2c), suggesting that infection stimulates distinct regulatory networks across epithelial cell types; for example, stem cells exhibited prominent increases in expression of genes linked to the MYC pathway, suggesting that infection triggers stem cell proliferation (Fig. 1d, Extended Data Fig. 2d). Highly induced genes in stem cells were generally different than those in most enterocyte populations and goblet cells (Fig. 1c, Extended Data Fig. 2e).

There were minimal differences in the relative abundances of epithelial clusters in the proximal SI in control vs infected animals (Extended Data Fig. 1b, 2f). In contrast, there was a marked increase in the abundance (12.6-fold) of cluster 5 enterocytes in the distal SI of infected animals (Fig. 1b, e). Cluster 5 enterocytes expressed the Reg3β and Reg3γ antimicrobial peptide genes even in the absence of infection (Extended Data Fig 3a), suggesting that this epithelial subset is specialized for defense against infection. With infection, cluster 5 enterocyte highly expressed genes classed as defense responses, including *Il18*, as well as genes encoding fibrinogen proteins, *Fga* and *Fgb*, which are traditionally associated with clotting[13] (Fig. 1f, Extended Data Fig 3a). In contrast, infection was associated with reduced expression of several metabolic pathways in this enterocyte subset (Extended Data Fig. 2c). Single molecule RNA FISH using probes for cluster 5 marker genes confirmed that these cells were found in the epithelium and that their abundance increased with infection; cluster 5 enterocytes were primarily located toward the base of the villus (Fig 1g and Extended Data Fig 3b), the site where *V. cholerae* primarily localizes as well[12].

Infection stimulated increased expression of *Reg3b* and *Reg3g* in all the epithelial cell clusters in the distal SI (Extended Data Fig 3a). Immunostaining established that Reg3β is highly expressed in epithelial cells towards the upper crypt and middle section of villi in infected animals (Fig. 1h, Extended Data Fig 3c). Moreover, Reg3β staining was often colocalized with *V. cholerae* microcolonies found on the epithelial surface (Fig.1h-j, Extended Data Fig 3c), suggesting that this lectin is secreted and bound to the pathogen during infection. Together, these analyses reveal that *V. cholerae* infection can shift the function of enterocytes towards defense both by reprogramming gene expression in many enterocyte subsets and by increasing the abundance of a defense-associated subset (cluster 5).

V. cholerae infection stimulates IL22 expression in type 3 innate lymphoid cells

Crosstalk between epithelial and immune cells found in the SI lamina propria plays a key role in host protection against enteric bacterial infection[9,14]. We also carried out scRNA-seq analysis of CD45+ immune cells isolated from the SI lamina propria of control and *V. cholerae*-infected P5 infant mice. Cell cluster analysis based on marker gene expression revealed 32 clusters in both the proximal and distal SI (Fig. 2a, Extended Data Fig. 4a-c, Supplementary Table 1). The cell types previously observed in adult animals[15] were also detectable in the SI of P5 neonates with the exception of plasma cells (Extended Data Fig. 4d). As observed for epithelial cell responses, there were more differentially expressed genes in the CD45+ cells isolated from the distal vs. proximal SI and considerable variability in infection-induced changes in gene expression among cell clusters (Fig. 2b, Extended Data Fig. 5a, Supplementary Table 4, 5). Pathway analysis revealed that, in contrast to scRNA-seq studies in *V. cholerae*-infected zebra fish, where the pathogen reduced interferon signaling in the intestine[16], interferon response

124 pathway genes were prominently induced in B and T cells, which express the receptors for Type
125 I (α and β) and II (γ) interferon, *Ifnar1/Ifnar2* and *Ifngr1/Ifngr2* respectively (Fig. 2bc, Extended
126 Data Fig. 5bc). NK cells may be the source of interferon gamma (Extended Data Fig. 5c), but
127 producer(s) of Type I and III (λ) interferon were not apparent.
128 Differential expressed gene (DEG) analyses uncovered that gene expression patterns in
129 Type 3 LTi-like innate lymphoid cell (LTi-like ILC3) are prominently altered by infection (Fig.
130 2b). Cell-cell communication inference[17] was used to identify potential signaling between lamina
131 propria LTi-like ILC3 and epithelial cells. Several pathways were inferred, including Il22-
132 Il22ra1/Il10rb signaling from LTi-like ILC3 to epithelial cells (Fig. 2e). We focused additional
133 analyses on Il22 signaling because this cytokine was highly up-regulated by *V. cholerae*
134 infection (> 16 fold increase, adjusted p-value 3.24×10^{-38}) (Supplementary Table. 5), and is
135 known to promote epithelial barrier integrity[18–22]. Flow cytometry analysis and whole mount
136 staining corroborated the increased number of Il22+ cells, which were primarily ILCs and not
137 γδT cells and found in the lamina propria and among intraepithelial lymphocytes (IEL) (Fig. 2fg,
138 Extended Data Fig. 5d). Quantitative PCR analysis with Il22 knockout animals confirmed that *V.*
139 *cholerae* infection-induced expression of *Reg3b* and *Reg3g* depends on IL22 signaling (Extended
140 Data Fig. 5e), as observed in studies with other enteric pathogens [19,23]. Furthermore, cluster 5
141 enterocyte marker genes induced by *V. cholerae* infection (Fig. 1g, Extended Data Fig. 3a) were
142 not induced in IL22 knockout mice (Fig. 2h), suggesting that Il22 signaling promotes the
143 generation of this defense-associated enterocyte subset.
144 Thus, similar to epithelial cell responses, transcriptional responses to *V. cholerae*
145 infection in lamina propria immune cells were cell type-specific and more pronounced in the
146 distal SI. Also, among lamina propria innate immune cells, increased ILC3 expression of
147 regulatory cytokines, including Il22, was notable.
148
149 **Il22 protects infant mice from *V. cholerae* intestinal colonization and diarrhea**
150 Since Il22 has been linked to intestinal defense[18–22] and transcriptional profiling
151 suggested that *V. cholerae* infection stimulates an Il22-based signaling axis between lamina
152 propria ILC3 cells and the epithelium, we investigated whether this cytokine could impact the
153 course of *V. cholerae* infection in suckling mice. Because of the low expression of Il22 in very
154 young animals[24], we speculated that the administration of exogenous Il22 could change the
155 outcome of *V. cholerae* infection in P5 animals. Infant animals were given two doses of an
156 IL22Fc protein[25] at 24 and 0 hours before challenge with *V. cholerae* (Fig. 3a). This prophylactic
157 regimen of IL22Fc administration markedly decreased the *V. cholerae* burden in both the
158 proximal and distal SI (Fig 3b, Extended data Fig. 6ab). In contrast, administration of
159 recombinant Il17a or Il17f, which were also activated in LTi-ILC3 by *V. cholerae* infection, or
160 Ifnβ or Ifnγ, whose receptor downstream signaling was activated in T, B and myeloid cells (Fig.
161 2bc, Extended data Fig. 5b), did not influence *V. cholerae* colonization (Extended data Fig. 6a-
162 d).
163 A bacterial-barcoding strategy was used to determine whether Il22-treatment strengthens
164 the initial bottleneck that limits *V. cholerae* colonization and/or prevents subsequent replication.
165 Amplicon sequencing and the STAMPR analytic pipeline monitor the diversity of otherwise
166 isogenic barcoded bacteria to quantify the number of cells that survive colonization bottlenecks
167 to initiate infection, referred to as the 'founding population'[26]. STAMPR revealed that both the
168 founding population (Ns) and net replication (CFU/Ns) in the distal SI were reduced in treated
169 animals (Fig. 3cd). These results suggest that IL22Fc both limits net replication and tightens the

host bottleneck, restricting the number of niches in the distal SI that are permissive for *V. cholerae* replication or killing cells before they become founders.

When *V. cholerae*-infected animals are left with a dam and monitored for survival, they develop diarrhea, lose weight, and generally die within 60 hours (Fig. 3e-g). In marked contrast, in animals treated with IL22Fc, no weight loss, diarrhea, or death was observed (Fig. 3e-g). In fact, the treated mice gained weight and at 60 hours had either entirely cleared *V. cholerae* or had dramatically lower pathogen burdens than observed in the moribund control animals (Fig. 3h). Only a single dose of IL22Fc 24 or 48 hours before infection was sufficient to impair *V. cholerae* colonization (Extended data Fig.6ab), while IL22Fc treatment 5 days prior to infection had limited effect (Extended data Fig. 6e). Administration of IL22Fc 5 hours post *V. cholerae* infection was sufficient to sustain the body weight of infant mice and prolong their survival, suggesting that this treatment could be beneficial even after infection (Extended data Fig.6fg). Together, these findings suggest that Il22 may have clinical value in preventing or even treating cholera.

We also tested whether prophylactic IL22Fc could reduce the colonization of other enteric pathogens in infant mice. IL22Fc markedly limited *Citrobacter rodentium* colonization in the SI and colon (Extended data Fig.6h). However, IL22Fc administration only led to a modest reduction in *Salmonella enterica* serovar Typhimurium intestinal colonization and did not reduce the pathogen burden in the liver or spleen (Extended data Fig.6i), suggesting that the treatment did not influence pathogen dissemination. These results suggest that IL22Fc treatment is particularly potent at impairing the intestinal colonization of extracellular pathogens in infant animals.

Elevated requirement for *V. cholerae* motility in Il22 treated animals

To understand how Il22-treatment alters the SI milieu, we compared *V. cholerae's* genetic requirements for intestinal colonization in Il22-treated and control mice using a transposon insertion site sequencing (Tn-seq) screen (Fig. 4a). In this genome-scale bacterial loss of function screen, comparisons of the abundances of transposon insertions in genes in the inoculum (input) to plated intestinal homogenates (output) are used to infer the genetic requirements for growth *in vivo*; reductions in the abundance of insertions in a gene in the output sample relative to the input suggests the gene promotes growth in the intestine. As expected, transposon insertions in genes encoding essential colonization factors, such as genes required for the biogenesis of the toxin-coregulated pilus (Tcp), were similarly depleted (compared to the inoculum) in both IL22Fc-treated and vehicle (PBS)-treated animals (Fig. 4b and Supplementary Table 6). In contrast, insertions in genes depleted more in IL22Fc-treated vs control animals compared to the inoculum represent genes that are more important for intestinal colonization in the IL22Fc-treated host. Notably, the relative depletion of insertions in 22 genes related to motility were 4-32x greater in IL22Fc-treated vs control animals (Fig 4b,c and Extended Data Table. 1), suggesting that motility is more important for *V. cholerae* colonization in IL22Fc-treated animals. Non-motile strains with deletions in genes important for flagellar assembly (*fliI* and *flgD*) and flagellar-based motility (*motB*)[27] were created, and competition assays against wild-type strains corroborated the heightened importance of motility in IL22Fc-treated mice (Fig. 4d). We hypothesized that the increased importance of motility for colonization in the IL22Fc-treated mice reflects the role of motility in *in vivo* pathogen localization. Consistent with this idea, the fraction of luminal vs tissue-associated *V. cholerae* (Fig. 4e,f) was ~86x greater in

216 the IL22Fc-treated mice, demonstrating that IL22Fc treatment alters the intestine in a manner
217 that impedes the pathogen from reaching the epithelial surface. In fact, it was difficult to detect
218 fluorescently tagged *V. cholerae* closely associated with the epithelium in the crypts of treated
219 mice (Fig. 4g). Together, these observations suggest that at least in part, IL22Fc treatment
220 restricts *V. cholerae* colonization by limiting the pathogen's access to the epithelial surface.
221
222 **IL22 administration modifies the gene expression profiles and cellular composition of the**
223 **SI epithelium**
224 Treatment with IL22Fc significantly increased the length of the SI, but not the colon,
225 without impacting the pups' body weight (Extended Data Fig. 7a-c), suggesting that this
226 cytokine modifies the development of the SI. 36 hours after IL22Fc administration, scRNA-seq
227 of the SI epithelium revealed a marked increase in the abundance of cluster 3 and 9 cells (Fig
228 5a,b, Supplementary Table 1). Moreover, IL22Fc treatment stimulated changes in the
229 transcriptomes of all types of epithelial cells in the distal SI (Extended Data Fig. 7d).
230 Unexpectedly, IL22Fc treatment reduced the expression of more genes than it increased in 13 of
231 14 clusters (Extended Data Fig. 7d, Supplementary Table 7). For some genes, IL22Fc
232 administration induced changes in all cell types (e.g. increased expression of antimicrobial
233 peptides) and in other cell subsets gene expression changes were more specific. For example, this
234 treatment only stimulated expression of pathways associated with cell cycle (Mitosis, E2F, and
235 MYC Target) in stem cells (Extended Data Fig. 7e). We confirmed stem cell proliferation in
236 IL22Fc-treated animals with EdU staining (Extended Data Fig. 7f-h), as reported[28]. There was
237 also a trend toward reduced expression of genes linked to lipid and sugar metabolism pathways
238 in enterocytes of IL22-treated mice, consistent with previous studies that elucidated a role of
239 IL22 signaling in metabolism (Extended Data Fig. 7i)[29]. Notably, in most enterocyte clusters,
240 genes highly expressed in cluster 5 enterocytes from *V. cholerae* infected animals were
241 prominently upregulated by IL22Fc-treatment (Fig. 5c), suggesting that IL22 reprograms
242 enterocytes to promote epithelial defense.
243
244 **IL22 induces expression of vibriocidal *Reg3b***
245 Among upregulated genes, pathway analysis revealed that IL22Fc increased expression
246 of genes linked to synthesis of antimicrobial peptides in all epithelial populations (Extended Data
247 Fig. 8a). *Reg3b* and *Reg3g* were among the most highly induced genes by Il22Fc treatment
248 (Extended Data Fig. 8a); IL22Fc treatment elevated expression of *Reg3b* and *Reg3g* 10,000-fold
249 compared to untreated animals, and ~10-fold compared to infected animals (Extended Data Fig.
250 8b). The elevated expression of these antimicrobial proteins, which was also associated with
251 IL22Fc treatment in a study of the colonic pathogen *Citrobacter rodentium* in adult mice[19], along
252 with *Defa24*, likely explains why antimicrobial pathways were one of the enriched pathways
253 associated with this treatment in all clusters (Extended Data Fig. 8b). Immunohistochemical
254 staining confirmed that Reg3β is expressed all along the crypt-villus axis in IL22Fc treated
255 animals (Extended Data Fig. 8c). Reg3β has been reported to kill several species of both Gram-
256 negative[30] and Gram-positive bacteria[31] *in vitro,* but susceptibility of *V. cholerae* to this lectin
257 has not been reported. In laboratory culture, we found that recombinant Reg3β decreased *V.*
258 *cholerae* survival in a dose-dependent fashion, whereas heat-inactivated Reg3β failed to kill *V.*
259 *cholerae* (Fig. 5d). Furthermore, oral administration of Reg3β recombinant protein decreased the
260 *V. cholerae* burden as well as the size of the founding population and pathogen proliferation
261 particularly in the distal SI (Fig. 5e-g), further confirming the vibriocidal activity of Reg3β *in*

262 *vivo*. P5 Reg3β$^{-/-}$ mice were as susceptible to *V. cholerae* intestinal colonization as heterozygous
263 littermates (Fig. 5h). However, IL22Fc administration to Reg3β$^{-/-}$ animals did not reduce the *V.*
264 *cholerae* burden, size of the founding population, or amount of net proliferation as potently as in
265 Reg3β$^{+/-}$ littermates (Fig. 5h-j), suggesting that the increased expression of Reg3β in IL22Fc
266 treated animals contributes to the protective effects of IL22 *in vivo*. Since Reg3β$^{-/-}$ animals were
267 still protected from *V. cholerae* infection by Il22Fc treatment (Fig. 5h), other protective
268 mechanisms beyond Reg3b induction likely exist.
269
270 **Il22 treatment increases the abundance of secretory epithelial cells**
271 IL22 signaling is thought to be important for Paneth cell maturation and maintenance[32,33].
272 In P5 animals, where Paneth cells are absent (Extended Data Fig. 1c), IL22Fc administration
273 increased the abundance of cluster 3 and 9 epithelial cells, which express *Atoh1* and *Spdef*, key
274 transcription factors for the differentiation of cells in the secretory lineage[34] that can further
275 differentiate into goblet cells, Paneth cells, enteroendocrine cells, or tuft cells. Based on marker
276 gene expression, including *Muc2* and the absence of *Lyz1* expression (Fig. 6ab), the cluster 3
277 epithelial subset resemble adult goblet cells rather than Paneth cells[35]. However, cluster 9 cells
278 have lower expression of other goblet cell marker genes and express stem cell markers (*Lgr5* and
279 *Olfm4*) (Fig. 6ab), suggesting this cluster can be classified as secretory progenitor cells[36]. RNA
280 FISH showed that cells expressing *Atoh1* and *Spdef* genes are primarily found in the crypts (Fig.
281 6c-e). Histologic assessment confirmed that there was an increased abundance of Muc2+ mucus-
282 containing (PAS+) cells in the crypts of IL22Fc treated mice (Fig. 6f-h). Together, these findings
283 suggest that IL22Fc treatment promotes the development of secretory lineage cells and goblet
284 cells *in vivo*.
285 Muc2 is the major gel-forming mucus protein expressed in goblet cells and secretory
286 lineage cells in the SI[37]. IL22Fc-treatment increased the abundance of mucus and Muc2 protein
287 in luminal contents (Fig. 6ij). Expression of glycosyltransferase, including *Mgat4c*, and *Fut2* was
288 also induced by IL22Fc-treatment, as well by *V. cholerae* infection (Extended Data Fig. 9ab).
289 Furthermore, modification of secreted Muc2 with fucose and *N*-acetylglucosamine was elevated
290 in treated mice (Extended Data Fig. 9c). Thus, IL22Fc administration elevates the abundance of
291 the Muc2+ cell population, as well as Muc2 secretion and modification.
292 To investigate if Muc2 plays a role in Il22 treatment mediated resistance to *V. cholerae*
293 colonization, we compared the effects of IL22Fc administration on *V. cholerae* colonization in
294 Muc2$^{-/-}$ and control (Muc2$^{+/+}$ or Muc2$^{+/-}$) littermates. Without IL22Fc administration, *V. cholerae*
295 colonization in Muc2$^{-/-}$ mice was comparable to that in control, with a modestly greater burden
296 (2.4-fold) in the distal SI of Muc2$^{-/-}$ mice. However, administration of IL22Fc had a much more
297 potent effect limiting *V. cholerae* colonization in both the proximal and distal SI in control vs
298 Muc2$^{-/-}$ mice; the Muc2$^{-/-}$ animals had a 817-fold (geometric mean) greater *V. cholerae* burden in
299 the proximal SI and 146-fold greater *V. cholerae* burden in the distal SI than control littermates
300 (Fig. 6j), suggesting that Muc2 contributes to the therapeutic activity of IL22Fc. Interestingly,
301 the role of Muc2 in mediating the activity of IL22Fc appears to be primarily in limiting the
302 pathogen's capacity to establish a colonization niche in the intestine (i.e., its founding population
303 size) rather than its proliferation (CFU/Ns) (Fig. 6kl). Overall, the increased importance of
304 flagellar-based motility for *V. cholerae* colonization in IL22Fc-treated animals found in the Tn-
305 seq screen (Fig. 4) is likely attributable to this cytokine's stimulation of Muc2 production, which
306 impedes pathogen access to its preferred niche along the epithelium in the crypts.
307

Discussion

Given the extreme rapidity of cholera progression, innate defenses are particularly critical for protecting humans against *V. cholerae*. Here, scRNA-seq profiling of epithelial and lamina propria immune cell responses to experimental cholera in infant mice uncovered new facets of mucosal defense in the small intestine and suggested that IL22-dependent mechanisms play a role in cholera defense. IL22 therapy was highly protective against *V. cholerae* colonization and diarrhea in infant mice. scRNA-seq profiling of IL22-treated animals offered new insights into the mechanisms of this cytokine and uncovered an IL22-stimulated shift in the pattern of intestinal epithelial cell differentiation toward the secretory cell lineage. The products of these cells, including Muc2, appear to be critical for IL22-mediated protection from experimental cholera, a mechanism that may generally contribute to the therapeutic effects of IL22 (Extended Data Fig. 10).

V. cholerae triggered changes in gene expression in most epithelial cell subsets but unexpectedly increased the abundance of an enterocyte subset (cluster 5) whose signature gene program was largely linked to defense. Since P5 mice lack Paneth cells, which are rich in antimicrobial peptides and are thought to protect the crypt stem cells[11], cluster 5 enterocytes may function in an analogous fashion during early life before Paneth cells arise around P15[11] . However, in contrast to Paneth cells, whose relative abundance undergoes a modest increase during acute infection[38], the abundance of cluster 5 enterocytes cells increased >10-fold during the 20 hours of exposure to *V. cholerae*. Because *V. cholerae* primarily localizes near the base of villi[12], our findings raise the possibility that a consequence of the pathogen's presence in the crypts is the stimulation of the differentiation of stem cells or transient amplifying cells into cluster 5 enterocytes, or enterocyte plasticity[39] could also contribute to increase the abundance of this mucosal defense-associated epithelial subset.

Several studies have revealed that IL22 deficient mice have heightened susceptibility to death from mucosal pathogens [18–20] . This work has led to the idea that IL22 promotes the integrity of the epithelium through a variety of mechanisms, including increases in antimicrobial proteins[19], epithelial cell surface modifications[24,40], and Paneth cell differentiation[32]. For enteric pathogens, such as *C. rodentium* and *C. difficile*, experimental infections in IL22-/- mice have not revealed marked increases in intestinal pathogen burdens[19,20,41], and heightened mortality has been attributed to dissemination of intestinal bacteria, at least in part due to reduced activity of complement C3[20]. Fewer studies have examined the consequences and the mechanisms of IL22 administration on pathogen burden. In adult mice *C. rodentium* infection, prophylactic administration of IL22Fc only modestly reduces colonic colonization, but significantly reduces disease by preventing epithelial damage[42].

In contrast, administration of IL22Fc almost entirely ablated the susceptibility of P5 mice to *V. cholerae* colonization. Several IL22-dependent mechanisms likely account for the marked reduction of *V. cholerae* colonization in IL22Fc-treated animals. Although there was a modest benefit to administering IL22Fc after infection, the most dramatic therapeutic effects of IL22Fc required that the cytokine be administered 24-48 hours before pathogen inoculation, indicating that time is required for the beneficial effects of IL22Fc to accrue. IL22Fc stimulated alterations in the transcriptional profile, cellular composition and even the length of the SI in P5 animals. One of the striking changes elicited by IL22Fc administration was the augmentation in expression of antimicrobial genes and additional defense-associated genes in most enterocyte subsets. For example, Reg3β became detectable in epithelial cells throughout the crypt-villus axis. However, since we found that the absence of Reg3β, in Reg3β$^{-/-}$ animals, did not render

354 mice more susceptible to *V. cholerae* colonization, physiologic levels of Reg proteins may be
355 insufficient to impede colonization. Instead, the supraphysiologic levels of Reg3β proteins and
356 other antimicrobial products induced by IL22Fc treatment likely are important for the beneficial
357 effects of IL22. Similarly, IL22 Fc administration markedly diminished colonic colonization
358 with *C. rodentium* in infant mice (Extended Data Fig. 6h), even though Reg3β$^{-/-}$ and Reg3γ$^{-/-}$
359 mice do not exhibit elevated pathogen burden or disease severity associated with this pathogen in
360 an adult mouse model[41,43].
361 The major mechanism underlying reduced *V. cholerae* colonization in IL22Fc-treated
362 animals is likely due to elevated Muc2 production. IL22Fc administration appears to drive the
363 differentiation of stem cells towards production of secretory cells *in vivo*, as suggested in
364 organoids[33]. IL22Fc administration did not elevate goblet cell numbers in adult mice[32],
365 suggesting that the mechanisms by which IL22 protects the host from infection may differ
366 according to age. Studies in suckling Muc2$^{-/-}$ mice revealed that IL22Fc administration was not
367 nearly as potent at impeding *V. cholerae* intestinal colonization as in littermate Muc2$^{+/-}$ controls.
368 Thus, mucin production appears to be required for robust IL22Fc activity. We propose that the
369 increase in goblet cell number and Muc2 secretion in IL22Fc treated animals blocks the pathogen
370 from reaching its preferred niche, where it establishes a founding population in close apposition
371 to the epithelium of the crypt[44,45] . The IL22Fc-stimulated impedance of pathogen access to the
372 epithelium and crypts likely explains the results of our TnSeq screen showing that flagellar-
373 based motility is especially important for pathogen colonization in the IL22Fc treated host.
374 Glycosylation of Muc2 may also modulate disease outcome by reducing cholera toxin
375 expression[46]. Finally, since mucus is decorated with glycans and antimicrobial proteins, and their
376 functions are entwined[47], the dramatic beneficial effects of IL22Fc on experimental cholera
377 likely derive from synergistic interactions between these components of innate intestinal defense.
378 Overall, the marked reduction in *V. cholerae* colonization likely explain the IL22Fc-mediated
379 protection from cholera-like death in suckling mice.
380 IL22 signaling in human responses to cholera have not been reported but activation of
381 IL1β and IL23, potent inducers of IL22-producing cells[48] has been inferred from studies of
382 duodenal biopsies from cholera patients[8]. Our findings suggest that investigation of the roles of
383 IL22 and IL22 gene polymorphisms in cholera clinical outcomes is warranted. Furthermore,
384 given the dramatic benefits of IL22Fc in the suckling mouse model of cholera and the emergence
385 of highly antibiotic-resistant *V. cholerae*[49], studies of this fusion protein as a prophylactic agent
386 for individuals susceptible to household contact infection[50] and/or as an adjunctive therapy
387 along with fluid resuscitation for cholera should be considered. Moreover, IL22Fc administration
388 maybe an important therapeutic adjuvant for other extracellular enteric pathogens such as
389 enterotoxigenic *E. coli,* another pathogen that like *V. cholerae*, does not damage the epithelium.
390 Several clinical trials have revealed the safety of IL22Fc in humans with dose-limiting adverse
391 events on skin when IL22Fc is administered repeatedly[25,51,52]. Since *V. cholerae* and ETEC are
392 particularly dangerous in young children, the safety of IL22Fc would need to be established in
393 this age group. Also, it would be valuable to study whether IL22Fc administration would be
394 beneficial in the epidemiologic conditions, such as undernutrition where cholera is prevalent.
395 Costs of this fusion protein could be prohibitive but alternative cheaper methods to promote
396 endogenous IL22 production such as tryptophan metabolites that promote ILC3 differentiation
397 and IL22 production[53] may be feasible.
398
399

Materials and Methods

Mice

C57BL/6NCrl (strain code: 027) dams with infant mice (P3-P4) were purchased from Charles River Laboratory or bred in the Bio Safety Level 1 (BSL1) animal facility in Brigham and Women's Hospital. Il22 knockout (C57BL/6-Il22tm1.1(icre)Stck/J; RRID:IMSR_JAX:027524) mice were from Jackson Laboratory (Bar Harbor, ME) and Muc2 knockout mice are gift from Anna Velcich(*57*). Reg3β knockout (C57BL/6NCrl-Reg3bem1(IMPC)Mbp/Mmucd, RRID:MMRRC_067360-UCD) was obtained from the Mutant Mouse Resource and Research Center (MMRRC) at University of California at Davis, an NIH-funded strain repository, and was donated to the MMRRC by Kent Lloyd, D.V.M., University of California, Davis.

Mice were maintained in a BSL1 animal facility at Harvard Medical School or Brigham and Women's Hospital and transferred to the BSL2 animal facility for the infection experiments. Animals were maintained in cages filled with pine wood bedding and paper nesting material with chow (LabDiet 5053) and water by the animal facility staff. All animal experiments were performed according to protocols reviewed and approved by the Brigham and Women's Hospital Institutional Animal Care and Use Committee (protocol 2016N000416) and in compliance with the Guide for the Care and Use of Laboratory Animals. Both male and female mice were mixed and randomly assigned to experimental groups.

Bacteria Strains and culture

A *Vibrio cholerae* O1 Ogawa clinical isolate from the 2010 Haiti outbreak (HaitiWT)[54] was used here. Motility deficient mutants *(ΔmotB, ΔflgD, ΔfliI*) were created using homologous recombination as described[55]. To create targeting vectors, 1000 bp of DNA flanking each side of the targeted genes were amplified with Phusion DNA polymerase (NEB) and these segments were cloned into pCVD442's SmaI site using NEBuilder HiFi DNA assembly kit (NEB). Barcoded WT or motility deficient mutants *V. cholerae* were generated as previously described[56]. Fluorescent protein tdTomato labeled HaitiWT was created previously[57]. Primers used for the plasmid construction are listed in supplementary data (Supplementary Table S8). A streptomycin resistant isolate of *Citrobacter rodentium* strain ICC168 and *Salmonella Enterica* Serovar Typhimurium SL1344 strain were also used.

In vivo infection and colony forming unit (CFU) counting

V. cholerae was cultured in lysogeny broth (LB) with streptomycin (Strep) 200 μg/mL at 37 °C overnight (~18 h) prior to animal experiments. Mice at postnatal day 5 (P5) (2.5-3.5 g of body weight) were infected with $1x10^5$ Vc^{STAMP} by oral gavage using PE-10 tubing. Weight and survival were monitored every 4-8 hours. and animals were euthanized when they lost 20% of body weight. 3 cm of proximal SI (samples were dissected after the gastro-duodenal junction) and distal SI (~3 cm from the end of the ileum) were homogenized with stainless beads in 33% glycerol LB. The homogenates were serially diluted and plated on LB Strep agar plates for CFU counting.

C. rodentium was cultured in LB media containing 200 μg/mL strep at 37 °C overnight (~24 h). P5 infant mice were infected with $1x10^8$ cells of *C. rodentium* by oral gavage using PE-10 tubing. Whole SI, and colon were dissected and homogenized in PBS and serial dilutions of the tissue homogenates were plated on LB Strep agar plates for CFU counting.

444 *S.* Typhimurium was cultured in LB Strep 200 μg/mL at 37 °C overnight prior to animal
445 experiments. P5 infant mice were infected with $1x10^7$ cells of *S.* Typhimurium by oral gavage
446 using PE-10 tubing. Infant mice were euthanized 1- or 3-days post infection. Whole SI, colon,
447 liver, and spleen were dissected and homogenized in PBS, and serial dilutions of the tissue
448 homogenates were plated on LB Strep agar plates for CFU counting.
449
450 **CD45+ immune cell isolation from small intestine lamina propria**
451 Infant mice were euthanized with isoflurane. Three centimeters of the proximal and distal
452 SI, as described above, were collected, cut open longitudinally, and stored separately in buffer
453 [2% Fetal Bovine Serum (FBS), 50 μg/mL Gentamicin (Gen), Penicillin-Streptomycin (PS)
454 PBS] on ice until all animals were dissected. Tissues were incubated in 10 mL of reducing buffer
455 [10 mM DTT 10 mM HEPES 2% FBS, 50 ug/mL Gen, PS, RPMI 1640], for 10 min on ice,
456 followed by incubation in 10 mL of epithelial dissociation buffer [5 mM EDTA, 10 mM HEPES,
457 2% FBS RPMI1640] at 37°C for 25 min. The remained tissue was washed in PBS, cut into small
458 pieces using dissection scissors, and incubated in digestion buffer [0.5 mg/mL collagenase D, 0.3
459 mg/mL Dispase II, 0.05 mg/mL DNase I, 10 mM HEPES 5% FBS, RPMI 1640] at 37°C for 30
460 min. After vortexing for 20 sec, dissociated tissue was passed through a 40 μm filter and
461 centrifuged at 300 xg for 5 min. The immune cells were further separated in a 40% /80% Percoll
462 gradient by centrifugation at 1900 xg for 30 min. The layer between 40% and 80% Percoll was
463 collected, mixed with 2% FBS 2mM EDTA PBS, and centrifuged at 300 xg for 5 min. Cells
464 were resuspended in 2% FBS 2mM EDTA PBS containing anti-CD16/32 antibody, and stained
465 with anti-CD45 FITC antibody. After being washed in 2% FBS 2mM EDTA PBS, cells were
466 stained with propidium iodide before sorting, and the CD45+ PI- population was isolated using a
467 cell sorter (SH800Z, Sony, Japan).
468
469 **Single-cell isolation of Epcam+ epithelial cell**
470 Infant mice were orally infected with 10^5 WT *V. cholerae* cells and euthanized 20 hpi.
471 For IL22Fc (Genentech)[25] treatment, P4 mice were administered 20 μg of IL22Fc
472 intraperitoneally and returned to their dam. After 36 hours, the mice were euthanized. Proximal
473 and distal SI were collected, cut open longitudinally, and washed in Gut wash media [2% FBS,
474 10 mM HEPES, 100 μg/mL Pen/Strep, 50 μg/mL gentamicin in RPMI1640] in 15 mL conical
475 tubes. Tissues were rinsed in ice-cold PBS, incubated in Epithelial dissociation solution [30 mM
476 EDTA in PBS] on-ice for 40 min, shaken gently 30 times every 5 min, and then vortexed for 20
477 seconds. Tissue pieces were removed with forceps. Dissociated cells in the supernatant were
478 centrifuged and resuspended in ice-cold PBS. This step was repeated twice to wash out EDTA.
479 The cell pellets were resuspended in Dispase solution [2% FBS, 0.1 mg/ml dispase in 4 ml
480 RPMI1640 per animal] at RT for 3-5 min, then cells were dissociated by pipetting with a wide-
481 bore tip, followed by pipetting 10 times with normal tips. 4 ml of ice-cold RPMI1640 containing
482 2% FBS was added to the cell suspension and filtered through a 70 μm cell strainer. The strainer
483 was washed with ice-cold RPMI1640 containing 2% FBS to collect the cells. Cells were pelleted
484 by centrifugation, stained with anti-Epcam FITC (1:100), and passed through a 100 mm cell
485 strainer. After being stained with LIVE/DEAD Fixable Violet Dead cell staining kit
486 (ThermoFisher, L34964), live Epcam+ cells were sorted by a SONY SH800Z Cell sorter.
487
488 **Single-cell RNA-Seq**

Sorted CD45+ SI lamina propria (LP) immune cells or Epcam+ epithelial cells were collected into PBS containing 2% FBS, followed by centrifugation at 1000 xg for 5 min, resuspended in PBS, counted, and passed through a 40 μm cell strainer. Single-cell suspensions were applied to a 10X Chromium Controller for GEM generation using Chromium Next GEM Single Cell 3' Reagent Kits v3.1 (10x Genomics). After barcoded cDNA generation, samples were amplified with the index primers (Dual Index Kit TT Set A, 10x Genomics) for 12 cycles. The libraries were sequenced on a NovaSeq 6000 S1 or NextSeq500. Data analysis was performed using 10x Cloud Analysis, and the filtered feature H5 files were used for further analysis with the Seurat package in R. Seurat objects were generated using Seurat v5.0.0 (https://satijalab.org/seurat/). Low-quality droplets (nFeature_RNA > 200 & nCount_RNA > 1000 & percent.mt < 20) and potential multiplets detected by scDblFinder were removed. Data from uninfected and infected proximal and distal SI samples were normalized by SCTransform (method = "glmGamPoi", vst.flavor = "v2") and integrated by Seurat's functions. Clustering was performed with Seurat's FindCluster (dims = 1:30, resolution = 0.4 for epithelial, 1.0 for CD45+ cells). Marker genes and differential gene expression analysis on each cell cluster was performed using the FindMarkers function of Seurat, and we annotated clusters based on canonical marker genes. Single-cell pathway analysis (SCPA) was performed by SCPA package v1.6.1 with default settings (downsample = 500, min_genes = 15, max_genes = 500) for epithelial cells, and downsample = 300 for CD45+ immune cells. Pathway enrichment was obtained by multiplying -1 to the fold change in the SCPA output. Pathways containing the following words were selected for coloring in Fig.1d: "INTERFERON" for IFN; "TNFA", "INFLAMMATORY", "INFLAMMATION" for TNFα, Inflammatory; "M_PHASE", "S_PHASE", "PRO_PHASE", "ANAPHASE", "CHROMATIDS", "G2_M_CHECKPOINTS", "SYNTHESIS_OF_DNA", "MITOTIC", "DNA_REPLICATION", "MYC", "E2F" for Mitosis; "TRANSLATION", "RIBOSOME", "RIBOSOMAL" for Translation and Ribosome; "GOLGI", "MTORC", "UNFOLDED", "HYPOXIA" for Golgi, ER, mTOR; "AMINO_ACID", "AMINO_ACIDS", "FATTY_ACID", "OXIDATIVE_PHOSPHORYLATION", "TCA_CYCLE" for Metabolism. For Fig.2b: "INTERFERON" for IFN; "IL17", "IL23", "PROINFLAMMATORY" for Proinflammatory, IL17, IL23; "TRANSLATION", "RIBOSOME", "RIBOSOMAL" for Translation, Ribosome; "GOLGI", "UNFOLDED", "MTOR", "HYPOXIA" for Golgi, ER, and mTOR. For Extended Data Fig.7e: "ANTIMICRO" for Antimicrobial peptides; "M_PHASE", "S_PHASE", "PRO_PHASE", "ANAPHASE", "CHROMATIDS", "G2_M_CHECKPOINTS", "SYNTHESIS_OF_DNA", "MITOTIC", "DNA_REPLICATION" for Mitosis; "TRANSLATION", "RIBOSOME", "RIBOSOMAL" for Translation and Ribosome; "E2F" for E2F; "MYC_" for MYC Target; "AMINO_ACID", "AMINO_ACIDS", "LIPID", "GLUCOSE", "SUGAR", "FATTY" for Lipid, Sugar, Amino acid. HALLMARK and KEGG pathways containing the following words were plotted in Extended Data Fig. 2c: "AMINO_ACID", "AMINO_ACIDS", "FATTY_ACID", "OXIDATIVE_PHOSPHORYLATION", "TCA_CYCLE".

Cell-cell communication analysis between epithelial and immune cells were performed using the CellChat package v2.2.0. First, epithelial and immune cell single cell RNA-seq data were integrated according to condition (uninfected or infected). Cellchat objects were generated using createCellChat function. Comparison of the communication probabilities mediated by ligand-receptor pairs from LTi-like ILC3 to enterocytes were performed by netVisual_bubble function and visualized by netVisual_chord_gene function with default settings.

535 **Flow cytometry**
536 SI lamina propria cells were isolated according to the protocol above. For intraepithelial
537 lymphocyte (IEL) isolation, distal SI tissue were cut open longitudinally and incubated in 10 mL
538 of reducing buffer [10 mM DTT 10 mM HEPES 2% FBS, 50 ug/mL Gen, PS, RPMI 1640], for
539 10 min on ice, followed by incubation in 10 mL of epithelial dissociation buffer [5 mM EDTA,
540 10 mM HEPES, 2% FBS RPMI1640] at 37°C for 25 min. After removal of the remaining tissue
541 pieces by pipetting, supernatants were passed through a 70 μm cell strainer and spun down at
542 300 xg for 5 min. The pellets were resuspended in 2 mL FACS buffer and overlayed onto
543 40%/80% Percoll gradients. Cells accumulated between 40% and 80% Percoll were transferred
544 to new tubes, washed in 5 mL of FACS buffer, and centrifuged at 500 xg for 5 min. Cell pellets
545 were washed in 2% RPMI1640 media and used for cell culture.
546 Cells isolated from LP and IEL were cultured in 10 % FBS RPMI1640 supplemented with 1x
547 Brefeldin A (Biolegend) and Penicillin/Streptomycin (Gibco) for 3 h. Cells were mixed with
548 anti-CD16/32 antibody (Biolegend, 101302) to block Fc binding, and stained with the following
549 combination of antibodies in 2% FBS 2mM EDTA PBS; Live/Dead Aqua (ThermoFisher,
550 L34957), anti-CD45+ Alexa Fluor 700 (BD Biosciences, 560510), anti-CD3e Super Bright 600
551 (ThermoFisher, 63-0031-82), anti-B220 FITC (Biolegend, 103206), anti-CD11b FITC
552 (Biolegend, 101206), anti-CD11c FITC (BD Biosciences, 557400), anti-TCRγ/δ APC
553 (Biolegend, 118143). After 30 min incubation at room temperature, cells were washed in 2%
554 FBS 2mM EDTA PBS and fixed in Fixation/ Permeabilization solution (ThermoFisher, 88-8824-
555 00) at 4 °C overnight. After washing, cells were stained with anti-IL22-PerCP-eFluor710
556 (ThermoFisher, 46-7222-80) at room temperature for 30 min and analyzed using a Cytek
557 Northern Light (Cytek, MA).
558
559 **Immunohistochemistry**
560 Distal small intestines were fixed in 4% paraformaldehyde (PFA) PBS for 4 hours and
561 dehydrated in 20% sucrose-PBS overnight. Tissue was embedded in OCT Compound: 20%
562 sucrose-PBS = 2.5:1 and frozen by liquid nitrogen. Tissue blocks were cut into 10 μm sections
563 with a cryostat at -18 °C (Leica) and the sections were dried at room temperature for 2h and
564 stored at -80 °C until use. Tissue sections were washed in PBS, blocked in blocking buffer [5%
565 goat serum 0.1% Triton X100 PBS] for 30 min, and stained with rabbit anti-Fga (1:100,
566 ProteinTech), rabbit anti-Fgb (1:100, ProteinTech), sheep anti-Reg3β antibody (1:100, R&D
567 Systems), rabbit anti-*V. cholerae* antisera Ogawa (1:100, BD Difco), and Ulex Europaeus
568 Agglutinin I (UEA-I) Fluorescein (1:100, Vector) at 4 °C overnight. Tissue sections were
569 washed in PBS twice and stained with anti-sheep IgG Alexa Flour 555 (1:200, ThermoFisher),
570 goat anti-rabbit IgG Alexa Flour 488 (1:200, ThermoFisher), or chicken anti-rabbit IgG Alexa
571 Flour 647 (1:200, ThermoFisher) and DAPI (1:1000, ThermoFisher) at room temperature for 30
572 min. The sections were washed in PBS and covered with Prolong gold antifade reagent
573 (ThermoFisher).
574 For PAS staining for paraffin sections, fixed tissue was processed, sectioned, and stained
575 at the Harvard Rodent Histology core. For Muc2 staining, paraffin sections were deparaffinized
576 with xylene for 10 min x2, rehydrated in 100%, 80%, 70%, 60% ethanol, and PBS for 5 min in
577 each solution. Sections were incubated with antigen retrieval buffer (citrate buffer, pH 6.0) and
578 microwaved for 10 min. Rehydrated tissue was blocked in blocking buffer for 30 min, stained
579 with rabbit anti-Muc2 antibody (1:100, Proteintech) in blocking buffer overnight, washed in
580 PBS, and stained with anti-rabbit IgG Alexa Flour 488 (1:200, ThermoFisher) at room

temperature for 30 min. The tissue was stained with DAPI, washed in PBS, and mounted in Prolong gold antifade reagent (ThermoFisher, P36934).

Fluorescent and PAS stain images were imaged with a Nikon Eclipse microscope with a Nikon Microscope Objective Plan Apo l 20x/0.75 OFN25 DIC N2 lens, Plan Flour 40x/1.30 Oil lens, or Plan Apo VC 100x/1.40 Oil DIC lens (Nikon) and captured with a Andor iXon DU-897E-CS0-#BV-500 Camera (Oxford Instruments).

Single molecule RNA Fluorescence *in situ* hybridization (RNAScope)

For detection of *Fgb* and *Sult6b2*, the dissected distal SI tissue was fixed in 4% PFA-PBS overnight at 4°C and dehydrated in 20% Sucrose-PBS overnight. Tissue was embedded in OCT Compound: 20% sucrose-PBS = 2.5:1 and frozen by liquid nitrogen. Tissue blocks were cut into 10 mm sections with a cryostat at -20 °C (Leica). The sections were attached to MAS coated slide glass (Matsunami), dried at -20°C for 2h and were stored at -80 °C until use. Tissue sections were stained according to the manufacture's RNAScope protocol (ACDbio) with hybridization probes: Mm-Sult6b2-C3 (1789851-C3) and Mm-Fgb-C2 (578921-C2). For detection of *Atoh1* and *Spdef*, P4 infant animals were administered PBS or 20 mg of IL22 and were returned to their dam. After 36 h, mice were euthanized, and tissues were processed as described above. Tissue sections were stained with hybridization probes Mm-Atoh1 (408791) and Mm-Spdef-C2 (544421-C2). Stained sections were imaged using a Nikon Eclipse microscope as above.

iDISCO clearing and 3D imaging

Two-centimeter pieces of distal small intestine were harvested from uninfected and infected animals and fixed in 4% paraformaldehyde PBS at 4°C overnight. Tissues were washed in PBS with 0.2% Tween-20 and 100 μg/mL Heparin for 1 hour twice and dehydrated gradually in 20%, 50%, 80% methanol (in PBS) for 1h, and twice in 100% methanol for 1h. Samples were then incubated overnight at room temperature on a shaker (50-60rpm) in 66% Dichloromethane (Sigma) /33% Methanol. Samples were then incubated with 5% H2O2 in 20%DMSO at 4'C overnight, and then washed in 100% methanol, then 20%DMSO/methanol, and then rehydrated with 80%, 60%, 50%, 40%, 20% methanol in PBS for 1h each, and PBS for 1h twice. Tissues were then permeabilized in 0.2% Triton X-100 at RT for 1h, and 0.2% Triton X-100/20% DMSO/0.3M Glycine for 1day at 37°C with gentle agitation. After being washed in 1X DPBS with 0.2% Tween-20 and Heparin (100 μg/ml) at RT for 1h twice, tissues were blocked in PBS with 0.2% TritonX-100/10% DMSO/6% Donkey Serum at 37°C with gentle agitation for 1 day, stained with rat anti-Il22 (1;100. Thermofisher) in PBS with 0.2% TritonX-100/10% DMSO/3% Donkey Serum at 4 °C for 2 days. The tissues were washed in wash buffer [PBS with 0.2%Tween-20, 100 μg/ml Heparin] for 30 min for 5 times, incubated with secondary antibody; anti-rabbit IgG Alexa 647 (1:200, Invitrogen), anti-rat IgG Alexa 568 (1:200, Invitrogen), and rabbit anti-Epcam Alexa 488 (1:100, Biolegend) in PBS with 0.2% TritonX-100/10%DMSO/6%Donkey Serum at 37C for 1 day. Samples were washed in wash buffer for 5 times, stained with 2μg/mL DAPI in PBS, washed in wash buffer for 5 times. To clear the tissue, samples were dehydrated with 20, 40, 50, 80, and 100% methanol and incubated in 66% DCM/33% methanol at room temperature for 3 hours, subsequently incubated in 100% dichloromethane at room temperature for 15 min twice, and incubated in 100% ethyl cinnamate. Tissues were placed on a glass bottom dish, and covered with100% ethyl cinnamate. Three dimensional images were captured using a confocal microscope (Stellaris 8 Falcon DIVA, Leica)

627 with Fluotar 16x/0.6 multi-immersion lense, and LasX acquisition software, built with arivis
628 Vision 4D software version 4.1.2 (Zeiss).
629
630 **Quantitative PCR**
631 Distal SI tissue from animals uninfected or infected with WT *V. cholerae* was collected at
632 20 hpi and homogenized in Trizol (ThermoFisher) with a bead beater with 3.2 mm metal beads.
633 Total RNA was isolated according to the manufactures' protocol. Total RNA was used for One-
634 step cDNA synthesis and qPCR with the Luna Universal One-Step RT-qPCR Kit (NEB,
635 E3005L) according to the manufacture's protocol. qPCR primer pairs are listed in
636 Supplementary Table 8.
637
638 **Sequence tag-based analysis of microbial population dynamics (STAMP)**
639 Infant mice were orally infected with barcoded Vc^{STAMP} and 16-20 hr later sacrificed and
640 tissue homogenates were plated for CFU counting as described above. The remaining SI
641 homogenates were plated on large (15cm diameter) LB-streptomycin plates and after overnight
642 culture at 37°C, cells were collected in 33% glycerol LB and stored at -20 °C. Two microliter of
643 each cell suspension was diluted with 100 µL milliQ water and boiled at 95 °C for 15 min. Each
644 sample was amplified with One Taq DNA polymerase, forward and reverse primers with unique
645 sequences that enable samples to be distinguished were used. The amplicons were purified using
646 the Genejet PCR purification kit and sequenced with NextSeq P1 100 cycle Reagent Kit
647 (Illumina). The barcode sequences were analyzed with STAMPR pipeline as described[26].
648
649 **Transposon insertion sequence (Tn-seq)**
650 A Tn-seq library in *V. cholerae* strain HaitiWT was used[58]. The library contained
651 ~195,000 distinct transposon insertions. Animals were intraperitoneally administered PBS
652 (control; n = 3) or IL22Fc (n=4) 24 h prior to infection. The transposon library was cultured in
653 25 mL of LB liquid media containing 200 µg/mL streptomycin and 50 µg/mL Kanamycin
654 (Strep/Kan) for 3 h at 37 °C with shaking. A higher inoculum size (~10^8 CFU) and lower dose of
655 IL22Fc (5 mg/animal) was used in these experiments compared to experiments described in Fig
656 3 to ensure that there would be sufficient numbers of CFU in intestinal homogenates to allow
657 statistically robust comparisons of the abundances of insertions in the inoculum with the
658 outputs[59] . Distal SI tissue was homogenized in 1mL of 33% glycerol LB and plated on LB
659 Strep/Kan agar plate and cultured at 37°C overnight. All colonies on those plates were harvested
660 in 2 mL of 33% glycerol LB and stored at -20°C until further processing. Genomic DNA
661 (gDNA) was extracted using gDNA extraction kit (Qiagen), sheared into 400 base pair (bp)
662 using Covaris, and was purified using the DNA clean kit (Qiagen). gDNA fragments were
663 repaired with Blunting enzyme mix (NEB), A-tails were added using Taq polymerase and dATP,
664 and ligated with adaptor sequences. Adaptor-ligated gDNA was amplified using Phusion PCR
665 polymerase with adaptor primers for 30 cycles. After purification, the amplicon was further
666 amplified with var primers and index barcodes. The amplified library with sizes between 300-
667 500 bp were isolated using SPRIselect beads (Beckman-Coulter). Sequencing was performed
668 using a Nextseq1000 with P1 100 cycle cartridge (illumina). Tn-seq data was analyzed using the
669 RTISAn pipeline as previously described[60].
670
671 **Competition assay with barcoded *V. cholerae***

672 Diluted WT or mutant *V. cholerae* STAMP libraries were cultured on 200 µg/mL
673 streptomycin LB (LB Strep) plates and 4-8 isolated colonies were picked. These single colonies
674 were then individually grown in LB Strep liquid media with shaking at 37 °C overnight; then
675 after adjusting OD600 to 1 with LB media, they were mixed in equal ratios. The barcoded strain
676 mix was stored as a glycerol stock at -80 °C until use.
677 P4 infant mice were intraperitoneally administered PBS or 5 mg IL22Fc 24 hours before
678 infection. The barcoded strain mix was cultured in LB Strep liquid media with shaking at 37 °C
679 overnight and infant mice were orally inoculated with $1x10^7$ cells of the strain mix and sacrificed
680 at 20 hpi. Homogenates of the distal SI tissue were plated on LB Strep plates, grown at 37 °C
681 overnight, and colonies were collected in 33% glycerol LB. Genomic DNA was extracted from
682 the collected bacteria and DNA barcodes were analyzed according to the protocol described
683 above. To calculate competitive indices, the frequency of each barcode in the output population
684 (from intestinal homogenates) was divided by the frequency in the inoculum. The geometric
685 mean of the resultant ratio of barcode frequencies (output/inoculum) in mutants were compared
686 to those of the WT strain in each individual mouse.
687
688 **Reg3β bactericidal assay *in vitro* and *in vivo***
689 An overnight culture of wild type *V. cholerae* was inoculated in LB Strep and incubated
690 at 37°C for 3 hours. The cell density (OD600) was adjusted to 0.1 (~10^8 cells/mL) and cells were
691 washed in MES buffer (100mM MES pH5.8, 25mM NaCl) twice. 10^5 cells were mixed with
692 recombinant Reg3β protein (Sino Biological) in MES buffer and incubated at 37°C for 3 h. Cells
693 were resuspended in LB media and either plated on LB Strep agar or growth was monitored in a
694 BioTek Epoc2 Microplate Spectrophotometer (Agilent, CA).
695 For *in vivo* assays, P5 infant animals were given 33.3ug of Reg3β protein orally 30 min
696 before and 1 hour after mice were orally gavaged with 10^5 cells of WT *V. cholerae*. Proximal
697 and distal SI tissues were harvested and homogenized in 33% glycerol LB at 16 hours post
698 infection. Serial dilutions of tissue homogenates were plated on LB Strep plates for CFU
699 counting.
700
701 **Proliferating cell staining with 5-ethynyl 2´-deoxyuridine (EdU)**
702 P4 infant littermate mice were randomly assigned to receive either PBS or IL22Fc. Mice
703 were administered 4 mg of EdU and PBS or 20 mg of IL22Fc intraperitoneally and returned to
704 their dam. After 36 hours, the mice were euthanized, dissected, and the SI tissue was fixed,
705 embedded, and cut into 10 mm cryosections as described above (See Immunohistochemistry).
706 Tissue sections were stained with Click-iT™ EdU Cell Proliferation Kit for Imaging, Alexa
707 Fluor™ 647 dye (ThermoFisher), according to the manufacture's protocol. Figure images were
708 captured with Nikon Eclipse microscope with Nikon Microscope Objective Plan Apo l 20x/0.75
709 OFN25 DIC N2 lens and an Andor iXon DU-897E-CS0-#BV-500 Camera (Oxford Instruments).
710
711 **Image analysis**
712 All images were analyzed using Fiji Software version 2.14.0
713 (https://imagej.net/software/fiji/).
714 Pearson's correlation coefficient of colocalization between Reg3β and *V. cholerae* were analyzed
715 using Coloc2 plugin (https://github.com/fiji/Colocalisation_Analysis). Z-stack images (0.3mm
716 distance per image) of colocalization between Reg3β and *V. cholerae* were captured with Nikon
717 Microscope Objective Plan Apo VC 100x/1.40 Oil DIC lens and 3D images were built using 3D

viewer plugin (https://github.com/fiji/3D_Viewer). *Atoh1*+, *Spdef*+, and EdU+ cells were counted using Find Maxima function with the same setting of Prominence across all compared images.

Immunoprecipitation and western blot for intestinal contents

The distal SI tissue was collected from control or IL22Fc-treated infant animals and cut open longitudinally. The tissue was incubated in 4 mL of wash buffer [1mM DTT PBS with protease inhibitor (Roche, 4693159001)] on ice for 10 min and vortexed for 20 seconds. After the removal of tissue pieces, intestinal washes were centrifuged at 100 xg for 1 min to remove the large pieces of intestinal contents. The supernatant was concentrated by centrifugation at 4000 xg with 3 kDa MWCO Amicon Ultra centrifugal filter unit for 1 hour. The volume of the concentrate was adjusted to 400 μL with wash buffer. Twenty microliter of intestinal wash was used for immunoprecipitation and western blot. An antibody against Muc2 (ProteinTech, 27675-1-AP) was mixed with Pierce Protein A/G Magnetic Beads (Pierce, 88802) in PBS for 1 hour and further mixed with intestinal wash in 500 μL of IP buffer [0.1% Tween 20 PBS with protease inhibitor] for 3 hours at 4 °C. Beads were washed in 1mL of IP buffer three times, mixed with SDS-PAGE loading buffer containing DTT (NEB, B7703S), and boiled at 95 °C for 5 min. SDS-PAGE (ThermoFisher, WG1403BOX) and transferring to nitrocellulose membrane (ThermoFisher. IB23001) were performed using iBlot 2 (ThermoFisher) according to manufactures' protocol. After blocking the membrane with 5% skimmilk TBST, the membrane was incubated with antibody against Muc2 (Abcam, EPR23479-47, 1:1000) in TBST at 4 °C overnight. After wash in TBST, the membrane was incubated with IRDye 800CW goat anti-rabbit IgG Secondary Antibody (LICORbio, 926-32211, 1:5000) and UEA-I Fluorescein (vector, FL-1061, 1:5000) at room temperature for 1 hour. After wash in TBST, the fluorescent signal was detected using ChemiDoc MP imaging system (Bio-rad).

Statistical Analysis

Statistical analysis was performed using Prism10 software version 10.4.0. For the CFU, founding population (Ns), and CFU/Ns comparison in animal infection studies, values were transformed to logarithm 10 before statistical analysis. n represents the number of animals unless otherwise noted in the figure legend.

Acknowledgments: We thank members of the Waldor lab for helpful comments on this project and manuscript and Franz Zingl Ph.D. for data in Fig. 5d. We thank Paula Montero Llopis, Ph.D., Praju Vikas Anekal, Ph.D., and Adrienne Wells, Ph.D. in the MicRoN Center at Harvard Medical School for histology, immunohistochemistry and 3D imaging, the Harvard Rodent Histology Core for tissue sectioning and staining, the Harvard Biopolymers facility for RNA sequencing, and the Harvard Research Computing Core for providing the computational analysis platform. We are grateful to Anna Velcich at College of Medicine/Albert Einstein Cancer Center for providing us Muc2 knockout mice, and to Genentech for providing us IL22-Fc recombinant protein.

Funding:

National Institutes of Health grant AI-042347 (M.K.W.)

Howard Hughes Medical Institute (M.K.W.)

Author contributions:
Conceptualization: M.S., Y.H., H. Z., M.K.W.
Methodology: M.S., Y.H., H. Z.
Investigation: M.S., Y.H.
Visualization: M.S., Y.H.
Funding acquisition: M.K.W.
Project administration: M.K.W.
Supervision: M.K.W.
Writing – original draft: M.S., Y.H., and M.K.W.
Writing – review & editing: M.S., Y.H., H. Z., M.K.W.

Competing interests: Authors declare there is no competing interests

Data and materials availability:

The data have been deposited in the NCBI Gene Expression Omnibus (GEO) database under accession number GSE288380.

Supplementary Materials

Extended Data Fig.1 to 10

Figures

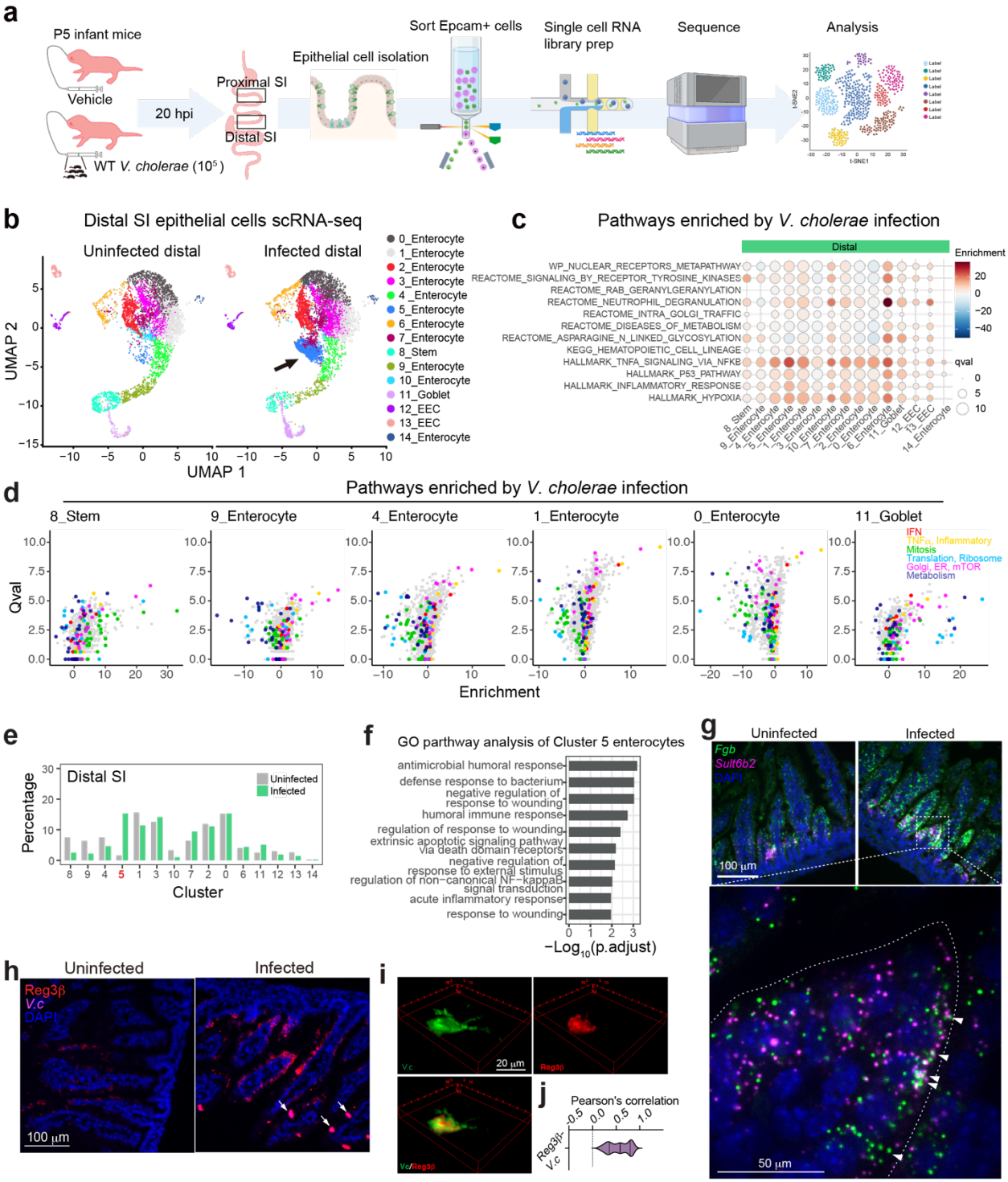

Figure 1. *V. cholerae* infection increases the abundance of cluster 5 enterocytes in the small intestine and elicits antimicrobial responses in intestinal epithelial cells in infant mice. **(a)** Experimental scheme of scRNA-seq analysis of epithelial cells. Infant mice (P5) (n=3/group) were infected with *V. cholerae* and sacrificed 20 hours post-infection (hpi). The proximal and

790 distal SI were collected, and epithelial cells were isolated. Single-cell RNA libraries were
791 prepared from sorted Epcam+ cells. **(b)** UMAP of the distal small intestine epithelial single-cell
792 RNA-seq data from uninfected and *V. cholerae* infected P5 infant mice (n=3 for each condition,
793 cells were pooled); EEC, enteroendocrine cells. The arrow indicates cluster 5 enterocytes in
794 infected animals in the distal SI. (**c**) Top-hit pathways from the Single Cell Pathway Analysis
795 (Qval > 8.75 in any cluster). Dot plot represents enrichment in color and Qval in circle size.
796 Stem, stem cells, EC, enterocytes, Gob, Goblet cells, EEC, enteroendocrine cells. (**d**) Volcano
797 plot showing q-value (Qval) and pathway enrichment from Single Cell Pathway Analysis.
798 Pathway enrichment indicates a mean pathway change comparing uninfected and *V. cholerae*-
799 infected conditions. Colors represent the following pathways: IFN (red), TNFα and
800 Inflammatory (yellow), Mitosis (green), Translation and Ribosome (light blue), Golgi, ER, and
801 mTOR (pink), and Metabolism (dark blue). (**e**) Percentage of cells in each cluster vs the total cell
802 number in the distal SI. (**f**) GO pathway analysis of cluster 5 representative genes. **(g)** *Fgb* and
803 *Sult6b2* gene detection by single molecule RNA FISH co-stained with DAPI (blue) in the distal
804 SI tissue at 20 hpi. White arrowheads in the higher magnification image indicate the expression
805 of *Fgb* (green) and *Sult6b2* (magenta) mRNA in epithelial cells. Dotted line indicates the
806 epithelial cell membrane. Signal intensity was adjusted to visualize single puncta in the high
807 magnification image. Color-separated images are shown in Extended Data. Fig.3b. (**h**)
808 Representative immunostaining of Reg3β (red), *V. cholerae* (magenta), and DAPI (blue) in the
809 distal SI from an uninfected animal (left) or *V. cholerae*-infected animal (right). Scale bar: 100
810 μm. White arrows show the colocalization of Reg3β and *V. cholerae* on the epithelium. (**i**)
811 Deconvoluted z-stack image of *V. cholerae* (green) and Reg3β (red) from a puncta of Reg3β/*V.*
812 *cholerae* colocalization image. Overlay image was taken by confocal microscope using x100
813 lens and z-stack with 0.3 micron gaps per layer. **(j)** Pearson's correlation coefficient between
814 Reg3β and *V. cholerae* co-localization using the images of (**h**) from infected animals. 55 images
815 from 4 animals were analyzed and plotted in a violin plot. (Fig. 1a is partially created in
816 https://BioRender.com.)
817
818
819
820

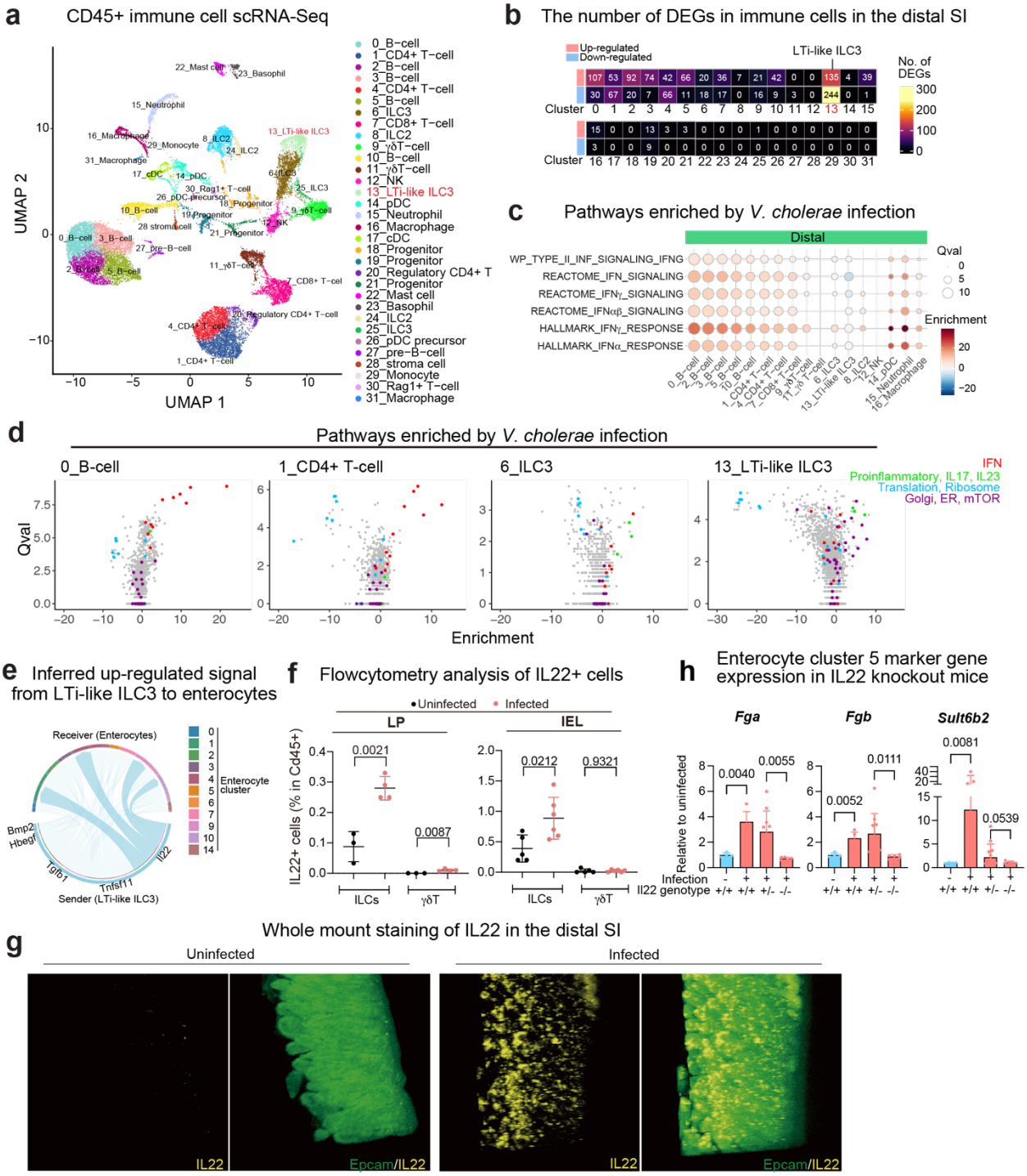

Figure 2. *V. cholerae* infection induces IL22 expression in Type 3 innate lymphoid cells. **(a)** UMAP of CD45+ immune cells (23,836 cells including all conditions: proximal and distal SI, mock and infected samples) in the lamina propria of the small intestine. **(b)** Heatmap of the numbers of differentially expressed genes (absolute Fold Change > 1, adjusted p-value < 0.00001, genes on chromosome X and Y were excluded as both, male and female infant mice were used for each condition, in each cluster). **(c)** Dot plots showing enrichment and Qval of the Single Cell Pathway Analysis results in color and circle size, respectively. Clusters with more than 500 cells (total cell number) isolated from distal SI are shown. **(d)** Volcano plots showing

830 enrichment and Qval of Single Cell Pathway Analysis results in the representative clusters for B
831 cells, T cells, and ILC3s. Colors represent pathways "Interferon" for IFN (red),
832 Proinflammatory, IL17, and IL23 (green), Translation and Ribosome (blue), Golgi, ER, and
833 mTOR (purple). **(e)** CellChat[17]-based analysis of up-regulated signaling pathways from LTi-like
834 ILC3 to enterocytes. Il22-Il22Ra1/Il10Rb signaling is highlighted. Color code represents the
835 types of enterocytes in the receiver. **(f)** Il22+ cell populations in Cd45+ cells in lamina propria
836 (LP, n = 3-4/group) and intraepithelial lymphocyte (IEL, n = 5-6/group). Data are represented as
837 mean ± SD for biological replicates. Unpaired t-test. Data are representative of two independent
838 experiments. **(g)** Whole mount staining of Il22 (yellow) and Epcam (green) in uninfected or
839 infected distal SI. Images are representative of three independent samples/group. (h) qPCR
840 analysis of cluster 5 enterocyte marker gene (*Fga*, *Fgb*, and *Sult6b2*) expression in the distal SI
841 from *V. cholerae* infected/uninfected WT C57BL/6 ($Il22^{+/+}$), infected $Il22^{+/-}$ and $Il22^{-/-}$ littermate
842 animals. Expression levels were normalized to β-Actin expression and shown as relative
843 expression to uninfected $Il22^{+/+}$ group.
844

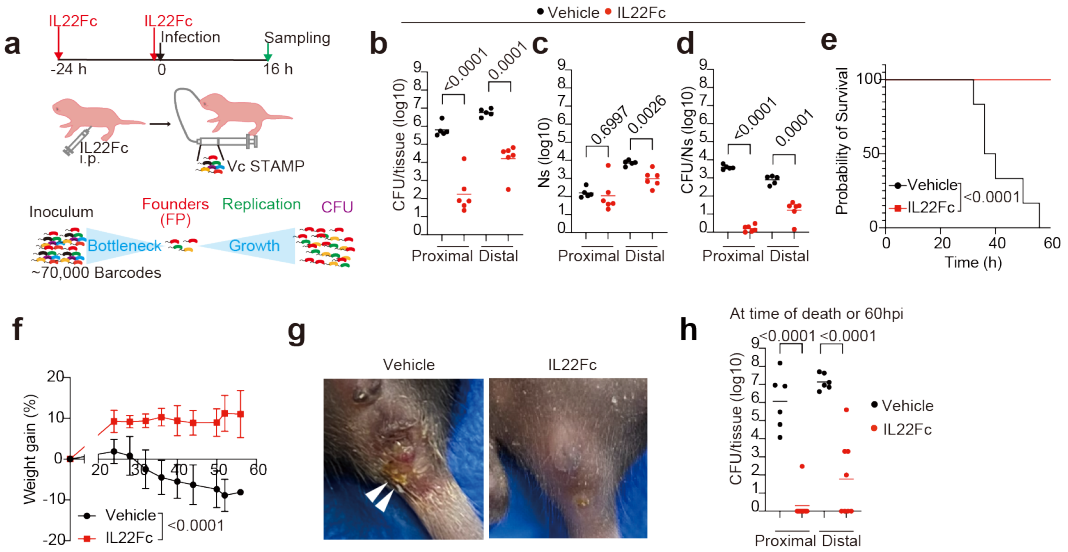

Figure 3. IL22 treatment protects infant mice from experimental cholera.
(a) Schematic of IL22 prophylactic regime. A barcoded library of *V. cholerae* was used in these experiments to enable measurement of the founding population (Ns), the number of cells from the inoculum that establish infection, and CFU/Ns which represents the net replication of the founders during infection. **(b-d)** CFU (b), founding population (Ns) (c), and replication (CFU/Ns) (d) of *V. cholerae* in the proximal and distal SI. Vehicle: PBS-treated animals, IL22Fc: IL22Fc-treated animals. Bars indicate the geometric mean for biological replicates (n = 5-6/group). Unpaired t-test. **(e)** Kaplan-Meyer plot of infant mice survival in *V. cholerae* infection in IL22Fc-treated or control animals; vehicle control (black, n = 6), IL22Fc-treated group (red, n = 8). Log-rank test. **(f)** Percent weight gain relative to the time of infection; vehicle (black, n = 6), IL22Fc-treated group (red, n = 8). Data are represented as mean ± SD. Two-way ANOVA. **(g)** Diarrhea in *V. cholerae*-infected infant mice at 48 hpi. White arrowheads in vehicle-treated animals point to clear diarrheal fluid on the anus. **(h)** *V. cholerae* burden in the proximal and distal SI at the time of death (vehicle-treated, black, n = 6) or 60 hpi (IL22Fc-treated, red, n = 8). Bars indicate the geometric mean. Unpaired t-test. P-values are shown.

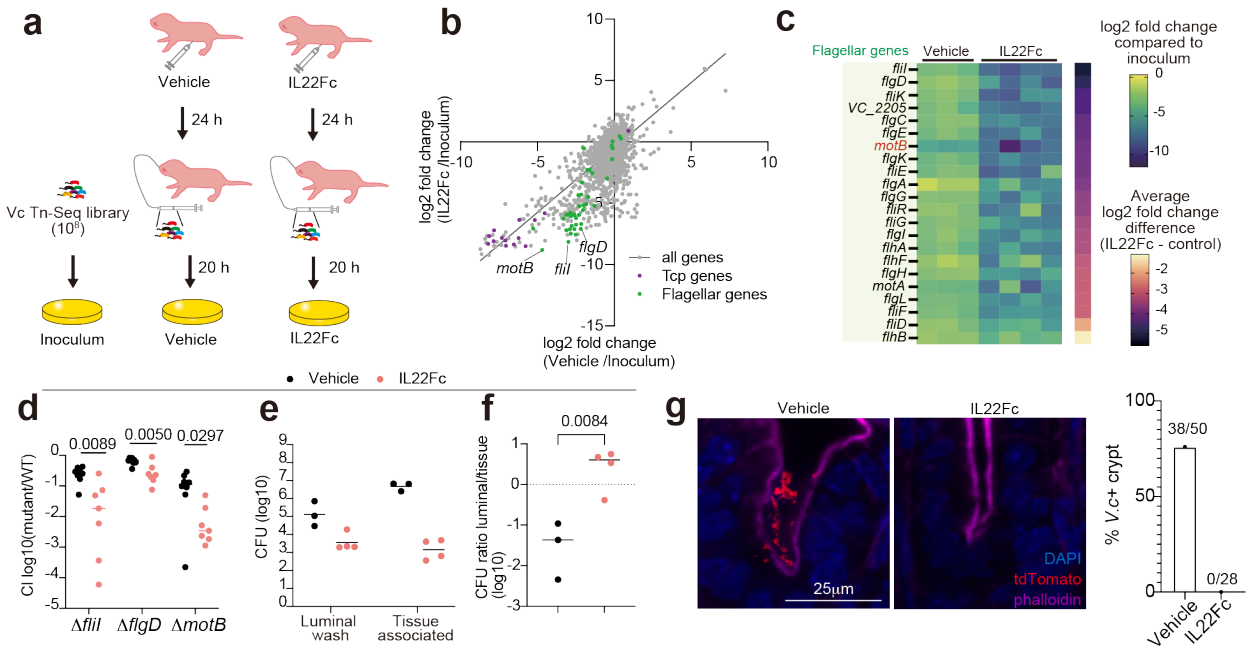

Figure 4. IL22Fc treatment modifies *V. cholerae* colonization requirements

(a) Experimental scheme of the transposon-insertion sequencing screen. Mice were given vehicle (PBS, n = 3) or 5µg of IL22Fc (n = 4) at 24 hours before infection and were infected with 10^8 cells of a *V. cholerae* transposon library. SI tissues were harvested at 20 hpi. **(b)** XY plot of transposon insertion frequency compared to inoculum (culture on LB plates); x-axis represents the mean of $\log_2$ fold change (bacteria recovered from distal SI of PBS-treated mice vs. inoculum) and y-axis represents the mean of $\log_2$ fold change (bacteria recovered from distal SI of IL22Fc-treated mice vs. inoculum). Purple dots: Tcp-biogenesis mutants; green dots: Flagellar-related mutants. The plot represents the mean value of biological replicates (Control: n = 3, IL22Fc: n = 4). **c)** Heatmap representing $\log_2$ fold change of transposon insertion frequency in flagellar genes in samples recovered from mouse tissue compared to inoculum. Column and row show individual mouse and *V. cholerae* genes, respectively. The magma color heatmap indicates the difference in the average of $\log_2$ fold change between IL22Fc-treated mice vs. control mice **(d)** Competitive index (CI) using barcoded mutant vs. WT strains in vehicle (black, n = 8) and IL22Fc-treated animals (red, n = 7). Multiple unpaired t-tests were performed between control vs IL22Fc-treated animals. Bars indicate the geometric mean, with the dotted line showing CI = 1. **(e)** CFU of *V. cholerae* detected in the luminal wash and attached to the tissue of the distal SI in vehicle-treated animals (black, n = 3) and IL22Fc-treated animals (red, n = 4). **(f)** Ratio of bacterial CFU in luminal washes compared with CFU of tissue-associated bacteria in vehicle-treated (black, n = 3) or IL22Fc-treated animals (red, n = 4). Unpaired t-test. **(g)** Representative images of WT *V. cholerae* colonization in the crypt in control animal (left image) and IL22Fc-treated animal (right image), and a bar graph showing the percent of crypts occupied by *V. cholerae* in the distal SI. Blue: DAPI, red: *V. cholerae LacZ::tdTomato*, magenta: phalloidin for actin staining. Scale bar: 25 µm. P-values are shown in individual figures.

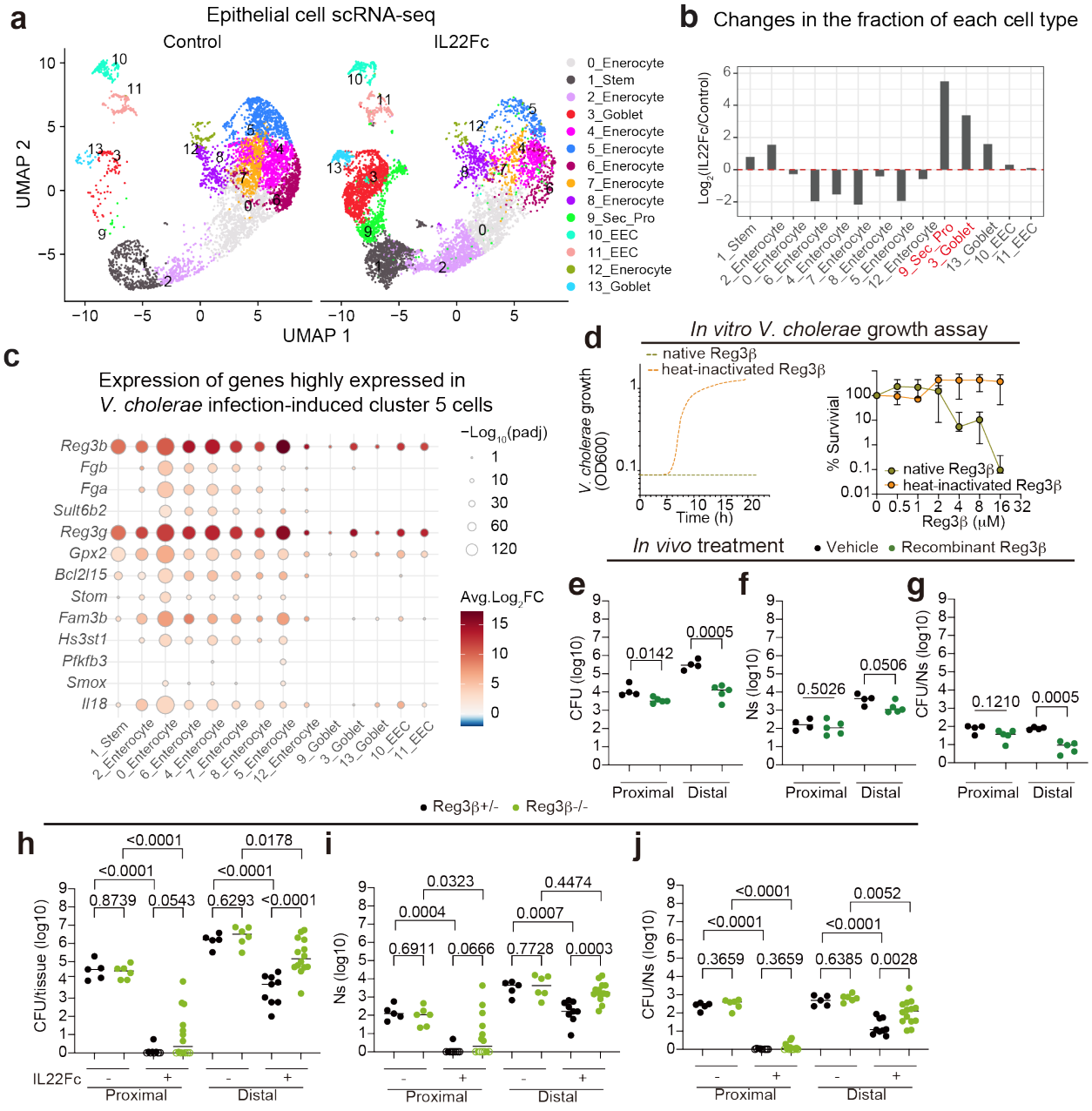

Figure 5. IL22Fc treatment alters intestinal epithelial cell transcriptional profiles. **(a)** UMAP of epithelial single-cell RNA-seq data of the distal small intestine in P5 infant mice in control and IL22Fc-treated animals. **(b)** Comparison of cluster abundance between IL22Fc-treated and untreated control animals. **(c)** Dot plot representing control vs. IL22Fc-treated gene expression changes of cluster 5 cell marker genes (Fig. S3A) in epithelial cell subsets. Color represents average $\log_2$ fold change of gene expression compared to untreated control. Dot size represents negative $\log_{10}$-scaled adjusted p-value. **(d)** *V. cholerae* growth curve measured by OD600 after incubation with native or heat-inactivated Reg3β (left). Percent *V. cholerae* survival after incubation with indicated concentration of Reg3β (right). Data represent mean ± SD for experimental replicates; native Reg3β (n = 4/condition), heat-inactivated Reg3β (n = 2/condition). **(e-g)** CFU (e), founding population (Ns) (f), and CFU/Ns (g) of *V. cholerae* in the

900 proximal and distal SI at 16 hpi. Infant mice were orally administered 2 doses of vehicle (PBS, n
901 = 4) or Reg3β recombinant protein (33 μg/dose, n = 5) at -0.5 and +1 hpi. Bars represent the
902 geometric mean for biological replicates. One-way ANOVA. (**h-j)** CFU (g), Ns (h), and CFU/Ns
903 (i) of *V. cholerae* in the proximal and distal SI of P5 Reg3β-/- mice and heterozygous littermate
904 at 16 hpi. Bars represent the geometric mean for biological replicates. Open circles indicate no
905 CFU detected. One-way ANOVA. Sample groups were compared among the same tissue. P-
906 values are shown.
907

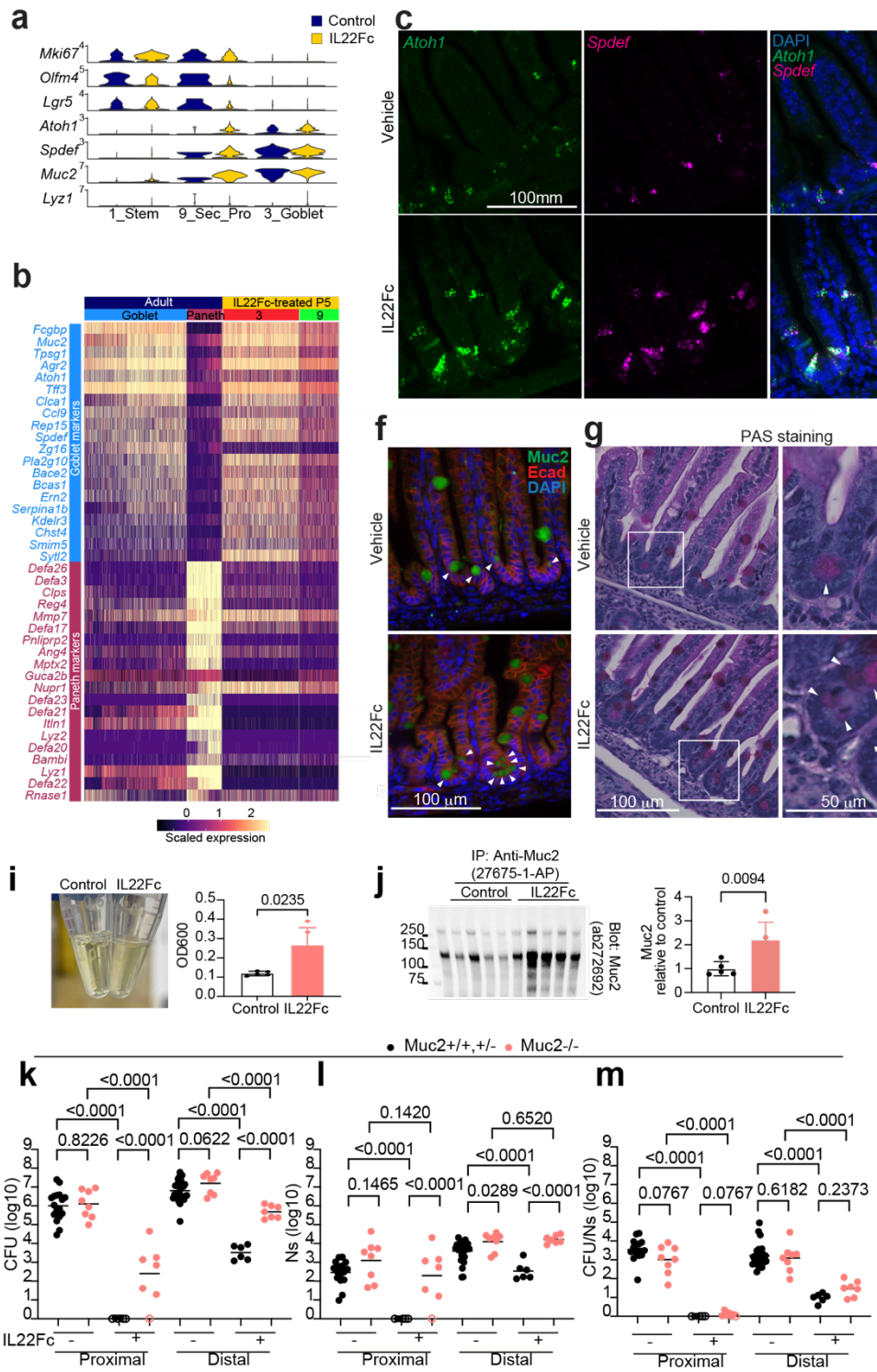

Figure 6. IL22Fc expands Goblet cells and Muc2 production is critical for IL22-mediated protection against *V. cholerae* colonization.

(a) Violin plot of traditional marker gene expression in stem cells, secretory progenitor cells, and goblet cells. *Lgr5* and *Olfm4*: stem cell marker, *Mki67*; proliferating cell marker, *Atoh1* and *Spdef*; secretory progenitor cell marker, *Muc2*: Goblet cell marker, *Lyz1*: Paneth cell marker. **(b)** Heatmap of goblet and Paneth cell marker expression in adult (Haber et al: GSE92332(*16*)) and

915 IL22Fc-treated P5 infant mice. (**c)** Representative RNAScope images of *Atoh1* (green) and *Spdef*
916 (magenta) expression in the epithelial cells in the crypts of the distal small intestine of vehicle-
917 and IL22Fc-treated infant mice. (**d, e)** The number of *Atoh1*+ (d), or *Spdef*+ (e) cells in the SI
918 epithelium. Vehicle: n = 122 images from 4 animals, IL22Fc: n = 141 images from 4 animals.
919 Unpaired t-test. (**f)** Representative images of immunohistochemistry of E-Cadherin (red), Muc2
920 (green), and DAPI (blue) in the distal small intestine of vehicle- and IL22Fc-treated animals.
921 White arrowheads point to the Muc2+ cells in the crypts. (**g)** PAS staining of the distal small
922 intestine of vehicle and IL22Fc treated animals. Arrowheads indicate PAS+ cells in the crypt.
923 Vehicle: n = 63 images from 3 animals, IL22Fc: n = 65 images from 3 animals. (**h)** Enumeration
924 of PAS+ cells in the crypts. Unpaired t-test with Welch's correction. (**i**) Western blot image of SI
925 luminal wash detected with anti-Muc2 antibody. n = 5/group. **(i)** Appearance of luminal washes
926 collected from control and IL22Fc-treated infant mice (left). Turbidity of luminal washes were
927 measured as OD600 in a spectrophotometer (right). **(j)** Immunoprecipitation-western blot for
928 Muc2 in luminal washes (right blot) and the signal intensity analyzed by densitometry (right bar
929 graph). Signal intensity was normalized by the average intensity in control samples. n =5/group.
930 (**k-m)** CFU (k), FP (l), and replication (CFU/FP) (m) of *V. cholerae* in the small intestine of P5
931 infant $Muc2^{-/-}$ vs littermate wild type or heterozygous controls ($Muc2^{+/+, +/-}$) animals treated with
932 (+) or without (-) IL22Fc. n = 6-28 animals/group. Bars represent the geometric mean for
933 biological replicates. One-way ANOVA. Sample groups were compared among the same tissue.
934 P-values are indicated in individual plots. Open circles indicate no CFU detected.
935

936 **References**
937

938 1. WHO. External Situation Report n. 22. *Multi-country outbreak of cholera* (2025).

939 2. Kanungo, S., Azman, A. S., Ramamurthy, T., Deen, J. & Dutta, S. Cholera. *The Lancet*
940 (2022).

941 3. Taylor, R. K., Miller, V. L., Furlong, D. B. & Mekalanos, J. J. Use of phoA gene fusions to
942 identify a pilus colonization factor coordinately regulated with cholera toxin. *Proc. Natl. Acad.*
943 *Sci.* **84**, 2833–2837 (1987).

944 4. Ryan, E. T. *et al.* Systemic, Mucosal, and Memory Immune Responses following Cholera.
945 *Tropical Medicine Infect Dis* **6**, 192 (2021).

946 5. Levine, M. M. *et al.* Duration of Infection-Derived Immunity to Cholera. *J. Infect. Dis.* **143**,
947 818–820 (1981).

948 6. Flach, C.-F. *et al.* Broad Up-Regulation of Innate Defense Factors during Acute Cholera.
949 *Infect. Immun.* **75**, 2343–2350 (2007).

950 7. Weil, A. A. *et al.* Posttranslational Regulation of IL-23 Production Distinguishes the Innate
951 Immune Responses to Live Toxigenic versus Heat-Inactivated Vibrio cholerae. *mSphere* **4**,
952 e00206-19 (2019).

953 8. Bourque, D. L. *et al.* Analysis of the Human Mucosal Response to Cholera Reveals Sustained
954 Activation of Innate Immune Signaling Pathways. *Infect. Immun.* **86**, 10.1128/iai.00594-17
955 (2018).

956 9. Kayama, H., Okumura, R. & Takeda, K. Interaction Between the Microbiota, Epithelia, and
957 Immune Cells in the Intestine. *The Annual Review of Immunology* (2020) doi:10.1146/annurev-
958 immunol-070119-115104.

959 10. Herrington, D. A. *et al.* Toxin, toxin-coregulated pili, and the toxR regulon are essential for
960 Vibrio cholerae pathogenesis in humans. *J. Exp. Med.* **168**, 1487–1492 (1988).

961 11. Lueschow, S. R. & McElroy, S. J. The Paneth Cell: The Curator and Defender of the
962 Immature Small Intestine. *Front Immunol* **11**, 587 (2020).

963 12. Millet, Y. A. *et al.* Insights into Vibrio cholerae Intestinal Colonization from Monitoring
964 Fluorescently Labeled Bacteria. *PLoS Pathog.* **10**, e1004405 (2014).

965 13. Luyendyk, J. P., Schoenecker, J. G. & Flick, M. J. The multifaceted role of fibrinogen in
966 tissue injury and inflammation. *Blood* **133**, 511–520 (2019).

967 14. Rogers, A. P., Mileto, S. J. & Lyras, D. Impact of enteric bacterial infections at and beyond
968 the epithelial barrier. *Nat. Rev. Microbiol.* **21**, 260–274 (2023).

969 15. Xu, H. *et al.* Transcriptional Atlas of Intestinal Immune Cells Reveals that Neuropeptide α-
970 CGRP Modulates Group 2 Innate Lymphoid Cell Responses. *Immunity* **51**, 696-708.e9 (2019).

971 16. Jones, L. O. *et al.* Single-cell resolution of the adult zebrafish intestine under conventional
972 conditions and in response to an acute Vibrio cholerae infection. *Cell Rep.* **42**, 113407 (2023).

973 17. Jin, S. *et al.* Inference and analysis of cell-cell communication using CellChat. *Nat Commun*
974 **12**, 1088 (2021).

975 18. Aujla, S. J. *et al.* IL-22 mediates mucosal host defense against Gram-negative bacterial
976 pneumonia. *Nat. Med.* **14**, 275–281 (2008).

977 19. Zheng, Y. *et al.* Interleukin-22 mediates early host defense against attaching and effacing
978 bacterial pathogens. *Nat. Med.* **14**, 282–289 (2008).

979 20. Hasegawa, M. *et al.* Interleukin-22 Regulates the Complement System to Promote Resistance
980 against Pathobionts after Pathogen-Induced Intestinal Damage. *Immunity* **41**, 620–632 (2014).

981 21. Nagao-Kitamoto, H. *et al.* Interleukin-22-mediated host glycosylation prevents Clostridioides
982 difficile infection by modulating the metabolic activity of the gut microbiota. *Nat. Med.* **26**, 608–
983 617 (2020).

984 22. Horn, V. & Sonnenberg, G. F. Group 3 innate lymphoid cells in intestinal health and disease.
985 *Nat. Rev. Gastroenterol. Hepatol.* **21**, 428–443 (2024).

986 23. Behnsen, J. *et al.* The Cytokine IL-22 Promotes Pathogen Colonization by Suppressing
987 Related Commensal Bacteria. *Immunity* **40**, 262–273 (2014).

988 24. Layunta, E., Jäverfelt, S., Dolan, B., Arike, L. & Pelaseyed, T. IL-22 promotes the formation
989 of a MUC17 glycocalyx barrier in the postnatal small intestine during weaning. *Cell Rep.* **34**,
990 108757 (2021).

991 25. Stefanich, E. G. *et al.* Pre-clinical and translational pharmacology of a human interleukin-22
992 IgG fusion protein for potential treatment of infectious or inflammatory diseases. *Biochem.*
993 *Pharmacol.* **152**, 224–235 (2018).

994 26. Hullahalli, K., Pritchard, J. R. & Waldor, M. K. Refined Quantification of Infection
995 Bottlenecks and Pathogen Dissemination with STAMPR. *mSystems* **6**, e00887-21 (2021).

996 27. Gardel, C. L. & Mekalanos, J. J. Alterations in Vibrio cholerae motility phenotypes correlate
997 with changes in virulence factor expression. *Infect. Immun.* **64**, 2246–2255 (1996).

998 28. Lindemans, C. A. *et al.* Interleukin-22 promotes intestinal-stem-cell-mediated epithelial
999 regeneration. *Nature* **528**, 560–564 (2015).

1000 29. Wang, X. *et al.* Interleukin-22 alleviates metabolic disorders and restores mucosal immunity
1001 in diabetes. *Nature* **514**, 237–241 (2014).

1002 30. Miki, T., Holst, O. & Hardt, W.-D. The Bactericidal Activity of the C-type Lectin RegIIIβ
1003 against Gram-negative Bacteria involves Binding to Lipid A*. *J. Biol. Chem.* **287**, 34844–34855
1004 (2012).

1005 31. Stelter, C. *et al.* Salmonella-Induced Mucosal Lectin RegIIIβ Kills Competing Gut
1006 Microbiota. *PLoS ONE* **6**, e20749 (2011).

1007 32. Gaudino, S. J. *et al.* IL-22 receptor signaling in Paneth cells is critical for their maturation,
1008 microbiota colonization, Th17-related immune responses, and anti-Salmonella immunity.
1009 *Mucosal Immunol.* **14**, 389–401 (2021).

1010 33. He, G.-W. *et al.* Optimized human intestinal organoid model reveals interleukin-22-
1011 dependency of paneth cell formation. *Cell Stem Cell* **29**, 1333-1345.e6 (2022).

1012 34. Yang, Q., Bermingham, N. A., Finegold, M. J. & Zoghbi, H. Y. Requirement of Math1 for
1013 Secretory Cell Lineage Commitment in the Mouse Intestine. *Science* **294**, 2155–2158 (2001).

1014 35. Peeters, T. & Vantrappen, G. The Paneth cell: a source of intestinal lysozyme. *Gut* **16**, 553
1015 (1975).

1016 36. Kolev, H. M. & Kaestner, K. H. Mammalian Intestinal Development and Differentiation—
1017 The State of the Art. *Cell. Mol. Gastroenterol. Hepatol.* **16**, 809–821 (2023).

1018 37. Johansson, M. E. V. & Hansson, G. C. Immunological aspects of intestinal mucus and
1019 mucins. *Nat. Rev. Immunol.* **16**, 639–649 (2016).

1020 38. Rodriguez, N. R. M. *et al.* Expansion of Paneth Cell Population in Response to Enteric
1021 Salmonella enterica Serovar Typhimurium Infection. *Infect. Immun.* **80**, 266–275 (2011).

1022 39. Meyer, A. R., Brown, M. E., McGrath, P. S. & Dempsey, P. J. Injury-Induced Cellular
1023 Plasticity Drives Intestinal Regeneration. *Cell. Mol. Gastroenterol. Hepatol.* **13**, 843–856 (2022).

1024 40. Goto, Y. *et al.* Innate lymphoid cells regulate intestinal epithelial cell glycosylation. *Science*
1025 **345**, 1254009 (2014).

1026 41. Melchior, K. *et al.* IL-22-dependent responses and their role during Citrobacter rodentium
1027 infection. *Infect. Immun.* **92**, e00099-24 (2024).

1028 42. Zhu, Q. *et al.* Epithelial dysfunction is prevented by IL-22 treatment in a Citrobacter
1029 rodentium-induced colitis model that shares similarities with inflammatory bowel disease.
1030 *Mucosal Immunol.* **15**, 1338–1349 (2022).

1031 43. Pham, T. A. N. *et al.* Epithelial IL-22RA1-Mediated Fucosylation Promotes Intestinal
1032 Colonization Resistance to an Opportunistic Pathogen. *Cell Host Microbe* **16**, 504–516 (2014).

1033 44. Campbell, I. W. *et al.* Vibrio cholerae motility is associated with inter-animal transmission.
1034 *Nat. Commun.* **16**, 7989 (2025).

1035 45. Bergstrom, K. S. B. *et al.* Muc2 Protects against Lethal Infectious Colitis by Disassociating
1036 Pathogenic and Commensal Bacteria from the Colonic Mucosa. *PLoS Pathog.* **6**, e1000902
1037 (2010).

1038 46. Wang, B. X. *et al.* Host-derived O-glycans inhibit toxigenic conversion by a virulence-
1039 encoding phage in Vibrio cholerae. *Embo J* **42**, e111562 (2023).

1040 47. Dupont, A., Heinbockel, L., Brandenburg, K. & Hornef, M. W. Antimicrobial peptides and
1041 the enteric mucus layer act in concert to protect the intestinal mucosa. *Gut Microbes* **5**, 761–765
1042 (2014).

1043 48. Bal, S. M., Golebski, K. & Spits, H. Plasticity of innate lymphoid cell subsets. *Nat Rev*
1044 *Immunol* **20**, 552–565 (2020).

1045 49. Rouard, C. *et al.* Long-Distance Spread of a Highly Drug-Resistant Epidemic Cholera Strain.
1046 *N. Engl. J. Med.* **391**, 2271–2273 (2024).

1047 50. Richterman, A., Sainvilien, D. R., Eberly, L. & Ivers, L. C. Individual and Household Risk
1048 Factors for Symptomatic Cholera Infection: A Systematic Review and Meta-analysis. *J. Infect.*
1049 *Dis.* **218**, S154–S164 (2018).

1050 51. Wagner, F. *et al.* Dose escalation randomised study of efmarodocokin alfa in healthy
1051 volunteers and patients with ulcerative colitis. *Gut* **72**, 1451–1461 (2023).

1052 52. Waters, M. *et al.* Astegolimab or Efmarodocokin Alfa in Patients With Severe COVID-19
1053 Pneumonia: A Randomized, Phase 2 Trial*. *Crit. Care Med.* **51**, 103–116 (2023).

1054 53. Shi, Z., Ohno, H. & Satoh-Takayama, N. Dietary Derived Micronutrients Modulate Immune
1055 Responses Through Innate Lymphoid Cells. *Front. Immunol.* **12**, 670632 (2021).

1056 54. Chen-Shan, C. *et al.* The Origin of the Haitian Cholera Outbreak Strain. *New Engl J Med*
1057 **364**, 33–42 (2011).

1058 55. Chao, M. C. *et al.* A Cytosine Methytransferase Modulates the Cell Envelope Stress
1059 Response in the Cholera Pathogen. *PLoS Genet.* **11**, e1005666 (2015).

1060 56. Fakoya, B. *et al.* Nontoxigenic Vibrio cholerae Challenge Strains for Evaluating Vaccine
1061 Efficacy and Inferring Mechanisms of Protection. *mBio* **13**, e00539-22 (2022).

1062 57. Leitner, D. R., Zingl, F. G., Morano, A. A., Zhang, H. & Waldor, M. K. The Mla pathway
1063 promotes Vibrio cholerae re-expansion from stationary phase. *mBio* **16**, e03433-24 (2024).

1064 58. Hubbard, T. P. *et al.* A live vaccine rapidly protects against cholera in an infant rabbit model.
1065 *Sci Transl Med* **10**, (2018).

1066 59. Chao, M. C., Abel, S., Davis, B. M. & Waldor, M. K. The design and analysis of transposon
1067 insertion sequencing experiments. *Nat. Rev. Microbiol.* **14**, 119–128 (2016).

1068 60. Hullahalli, K. & Waldor, M. K. Pathogen clonal expansion underlies multiorgan
1069 dissemination and organ-specific outcomes during murine systemic infection. *eLife* **10**, e70910
1070 (2021).

1071 61. Andreatta, M. & Carmona, S. J. UCell: Robust and scalable single-cell gene signature
1072 scoring. *Comput. Struct. Biotechnol. J.* **19**, 3796–3798 (2021).

1073 62. Haber, A. L. *et al.* A single-cell survey of the small intestinal epithelium. *Nature* **551**, 333–
1074 339 (2017).

1075 63. Schaum, N. *et al.* Single-cell transcriptomics of 20 mouse organs creates a Tabula Muris.
1076 *Nature* **562**, 367–372 (2018).

1077 64. Franzén, O., Gan, L.-M. & Björkegren, J. L. M. PanglaoDB: a web server for exploration of
1078 mouse and human single-cell RNA sequencing data. *Database* **2019**, baz046 (2019).

1079 65. Koprivica, I. *et al.* ILC3: a case of conflicted identity. *Front. Immunol.* **14**, 1271699 (2023).

1080 66. Scott, C. L., Bain, C. C. & Mowat, A. M. Inflammation, Methods and Protocols. *Methods*
1081 *Mol. Biol.* **1559**, 223–239 (2017).

1082 67. Vivier, E. *et al.* Innate Lymphoid Cells: 10 Years On. *Cell* **174**, 1054–1066 (2018).

1083 68. Parker, A. *et al.* Cell proliferation within small intestinal crypts is the principal driving force
1084 for cell migration on villi. *FASEB J.* **31**, 636–649 (2017).

1085